NAVAL POSTGRADUATE SCHOOL

MONTEREY, CALIFORNIA

THESIS

SOUND PROPAGATION CONSIDERATIONS FOR A DEEP-OCEAN ACOUSTIC NETWORK

by

Scott R. Thompson

December 2009

Thesis Advisor:	Joseph A. Rice
Co-Advisor:	John A. Colosi

Approved for public release; distribution is unlimited

REPORT DOCUMENTATION PAGE			Form Approved OMB No. 0704-0188
Public reporting burden for this collection of information is estimated to average 1 hour per response, including the time for reviewing instruction, searching existing data sources, gathering and maintaining the data needed, and completing and reviewing the collection of information. Send comments regarding this burden estimate or any other aspect of this collection of information, including suggestions for reducing this burden, to Washington headquarters Services, Directorate for Information Operations and Reports, 1215 Jefferson Davis Highway, Suite 1204, Arlington, VA 22202-4302, and to the Office of Management and Budget, Paperwork Reduction Project (0704-0188) Washington DC 20503.			
1. AGENCY USE ONLY ***(Leave blank)***	**2. REPORT DATE** December 2009	**3. REPORT TYPE AND DATES COVERED** Master's Thesis	
4. TITLE AND SUBTITLE Sound Propagation Considerations for a Deep-Ocean Acoustic Network		**5. FUNDING NUMBERS**	
6. AUTHOR(S) Scott R. Thompson			
7. PERFORMING ORGANIZATION NAME(S) AND ADDRESS(ES) Naval Postgraduate School Monterey, CA 93943-5000		**8. PERFORMING ORGANIZATION REPORT NUMBER**	
9. SPONSORING /MONITORING AGENCY NAME(S) AND ADDRESS(ES) N/A		**10. SPONSORING/MONITORING AGENCY REPORT NUMBER**	
11. SUPPLEMENTARY NOTES The views expressed in this thesis are those of the author and do not reflect the official policy or position of the Department of Defense or the U.S. Government.			
12a. DISTRIBUTION / AVAILABILITY STATEMENT Approved for public release; distribution is unlimited		**12b. DISTRIBUTION CODE**	

13. ABSTRACT (maximum 200 words)

The deep ocean is characterized by sound propagation that can support wide-area surveillance through the use of distributed acoustic sensors near the seabed. Such a deep-water sensor network is potentially enabled by phenomena such as Reliable Acoustic Path (RAP) and Deep Sound Channel (DSC) through which undersea network nodes can transmit and receive data across long distances. To provide a theoretical understanding of system effectiveness, the Bellhop acoustic modeling program is used to predict sensor coverage and communications range.

14. SUBJECT TERMS Acoustic Modem, Deep Water, Transmission Loss, Munk, Reliable Acoustic Path, RAP, Deep Sound Channel, DSC, Seaweb, Acoustic Communications, Acomms.			**15. NUMBER OF PAGES** 82
			16. PRICE CODE
17. SECURITY CLASSIFICATION OF REPORT Unclassified	**18. SECURITY CLASSIFICATION OF THIS PAGE** Unclassified	**19. SECURITY CLASSIFICATION OF ABSTRACT** Unclassified	**20. LIMITATION OF ABSTRACT** UU

NSN 7540-01-280-5500 Standard Form 298 (Rev. 2-89)
Prescribed by ANSI Std. 239-18

THIS PAGE INTENTIONALLY LEFT BLANK

Approved for public release; distribution is unlimited

SOUND PROPAGATION CONSIDERATIONS FOR A DEEP-OCEAN ACOUSTIC NETWORK

Scott R. Thompson
Lieutenant, United States Navy
B.S., United States Naval Academy, 2000

Submitted in partial fulfillment of the
requirements for the degree of

MASTER OF SCIENCE IN APPLIED PHYSICS

from the

NAVAL POSTGRADUATE SCHOOL
December 2009

Author: Scott R. Thompson

Approved by: Joseph A. Rice
Thesis Advisor

John A. Colosi
Co-Advisor

Andres Larraza
Chairman, Department of Physics

THIS PAGE INTENTIONALLY LEFT BLANK

ABSTRACT

The deep ocean is characterized by sound propagation that can support wide-area surveillance through the use of distributed acoustic sensors near the seabed. Such a deep-water sensor network is potentially enabled by phenomena such as Reliable Acoustic Path (RAP) and Deep Sound Channel (DSC) through which undersea network nodes can transmit and receive data across long distances. To provide a theoretical understanding of system effectiveness, the Bellhop acoustic modeling program is used to predict sensor coverage and communications range.

THIS PAGE INTENTIONALLY LEFT BLANK

TABLE OF CONTENTS

THIS PAGE INTENTIONALLY LEFT BLANK

LIST OF FIGURES

LIST OF TABLES

THIS PAGE INTENTIONALLY LEFT BLANK

LIST OF ACRONYMS AND ABBREVIATIONS

AcTUPℓ	Acoustic Toolbox User-interface & Post-processor
BPR	Bottom Pressure Recorders
DART	Deep-ocean Assessment and Reporting of Tsunamis
DI	Directivity Index
DSC	Deep Sound Channel
ISI	Inter-symbol Interference
MOST	Method of Splitting Tsunamis
NOAA	National Oceanic and Atmospheric Administration
NL	Noise Level
RAP	Reliable Acoustic Path
SBIR	Small-Business Innovative Research
SL	Source Level
SNR	Signal-to-Noise Ratio
SOFAR	Sound Fixing And Ranging
SOSUS	SOund Surveillance System
SSP	Sound Speed Profile
TWC	Tsunami Warning Center
TL	Transmission Loss
USV	Unmanned Surface Vehicle
UUV	Unmanned Undersea Vehicle

THIS PAGE INTENTIONALLY LEFT BLANK

ACKNOWLEDGMENTS

I would like to thank the following people for their assistance in writing this thesis:

First, to my wife Kelly, for without which I would not be as successful as I am today.

To my thesis advisors, Joseph Rice and John Colosi, for their guidance and encouragement while writing this thesis. Sensor/modem apparatus concepts and drawings for Seaweb and Deep Seaweb were provided by Joseph Rice.

To Harry Cox, whose topic suggestions helped guide my thesis research.

THIS PAGE INTENTIONALLY LEFT BLANK

I. INTRODUCTION

Traditional undersea acoustic surveillance systems such as the SOund Surveillance System (SOSUS) [1] require expensive and vulnerable electrical cables to connect sensors to shore sites where the data can be processed. Surveillance sensors could instead use acoustic modems to transport data. An acoustic network can move sensor data across long distances through a series of acoustic modems to a gateway node such as an Unmanned Surface Vehicle (USV) or surface buoy. The data then can be telemetered via satellite to remote locations for further evaluation. Persistent sound propagation features such as Reliable Acoustic Path (RAP) and Deep Sound Channel (DSC) channel can be exploited in the design of a deep-ocean sensor network.

This thesis provides a theoretical analysis of the potential for a deep-water acoustic network's effectiveness. The Bellhop acoustic modeling program predicts system characteristics such as effective range for various communication frequencies and source/receiver depths.

THIS PAGE INTENTIONALLY LEFT BLANK

II. BACKGROUND

Acoustic modems allow operators on the shore to remotely monitor deep ocean phenomena. For example, the Deep-ocean Assessment and Reporting of Tsunamis (DART) system aids the National Oceanic and Atmospheric Administration's (NOAA) ability to remotely monitor pressure events near the ocean bottom uniquely associated with a passing tsunami wave. In addition, the U.S. Navy's Seaweb system has demonstrated communications to and from sensors, Unmanned Undersea Vehicles (UUVs), and submarines in shallow water less than 300 meters. Deep-ocean environmental characteristics suggest the possibility of extending Seaweb functionality beyond the littoral and into the deep sea basins.

A. DART TSUNAMI WARNING SYSTEM

Tsunami detection capability gained attention with the December 26, 2004 tsunami near Indonesia. After this devastating event, which caused the deaths of over 300,000 people, the enhancement of NOAA capabilities was desired to "forecast the impact of tsunamis on coastal areas in time to save lives and protect property" [2] worldwide. One of the results was the expansion of the seven-node DART system into the 39-node DART II system. The technological advancement and increased coverage from DART to DART II help provide "a critical portion of NOAA's tsunami forecast, warning, and mitigation system" [2].

The DART II components and operation are illustrated in Figure 1. The system begins with the Bottom Pressure Recorders (BPR) scattered on the seabed throughout the deep ocean at stations shown in Figure 2. Upon sensing a spike in pressure exceeding some detection threshold, the BPR sends a report via acoustic modem to a moored buoy on the surface. The buoy transmits the report via Iridium satellite to a Tsunami Warning Center (TWC). At the TWC, the detection is further evaluated using the MOST (Method of Splitting Tsunamis) method to predict the likelihood and effects of a tsunami

occurrence. The information is then distributed to the public as a tsunami warning or general information. The DART II system was completed in March 2008.

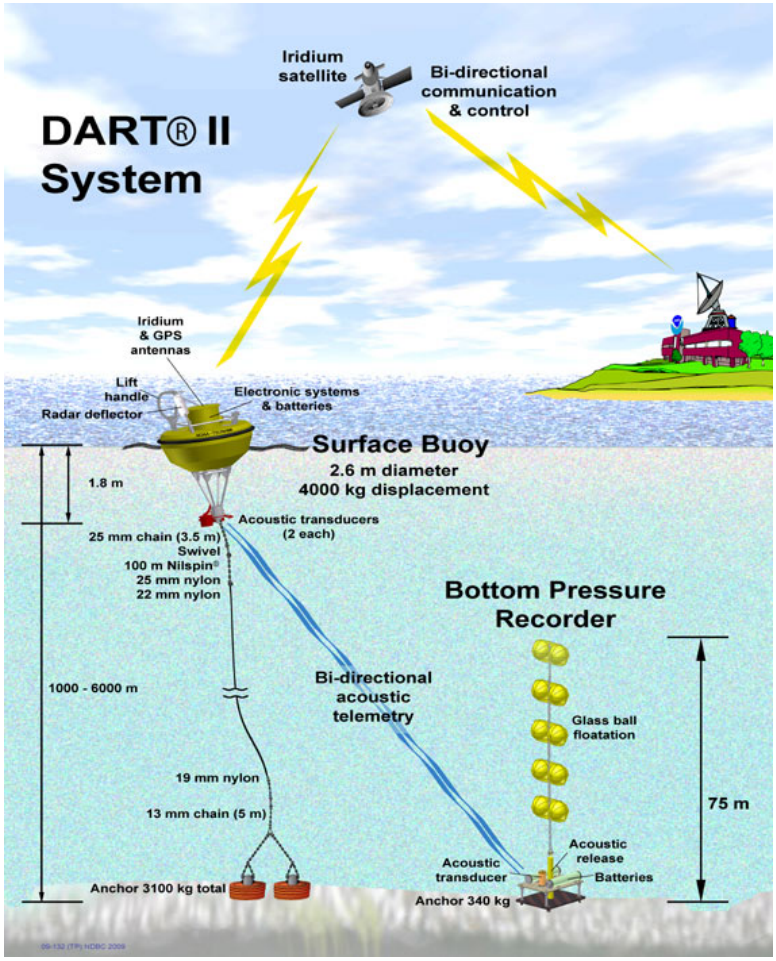

Figure 1. NOAA DART II system [From 3]

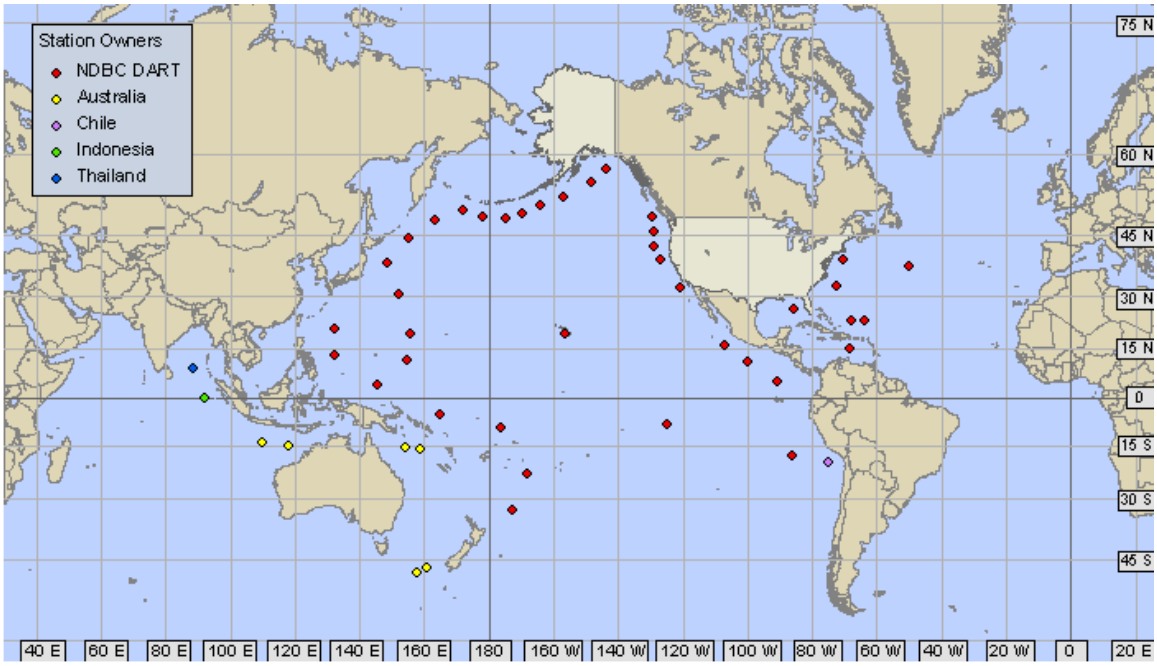

Figure 2. NOAA DART station [From 4]

The DART II acoustic modems provide for two-way communications between the moored buoy and BPR "to allow for two way transmission on demand" for the "measurement and reporting of tsunamis with amplitude below the auto-reporting threshold" [2]. The amount of data the BPR sends can be controlled to help meet the requirement for "very long life with few batteries, and an absolutely guaranteed transfer of sensor data into the modem, ready for transmission" [5]. Although the DART II "application does not require the transmission of large volumes of data nor does it require high data rates" [5], the ability to send only the most crucial information from the bottom of the ocean is adequate for tsunami warning.

B. SHALLOW SEAWEB

The acoustic modems employed in the DART II system are the product of a U.S. Navy Small-Business Innovative Research (SBIR) contract with industry. Using the same modems, the Navy has deployed over 50 Seaweb networks around the world in waters up to 300 meters deep. The Seaweb system begins with a sensor or undersea vehicle (such as a submarine) sending and receiving messages through an acoustic modem. The messages

are transmitted acoustically over the network of modems to a gateway node at the sea surface that can further relay, via satellite, the message to the shore or another ship. Two-way communications are available and the modems been shown to "effectively communicate with a ±30 kt platform operating with a modem designed for a standard 9-14 kHz band" [5]. Although Seaweb has the potential for use in the deep ocean, efforts to date have been limited to using the system in littoral environments.

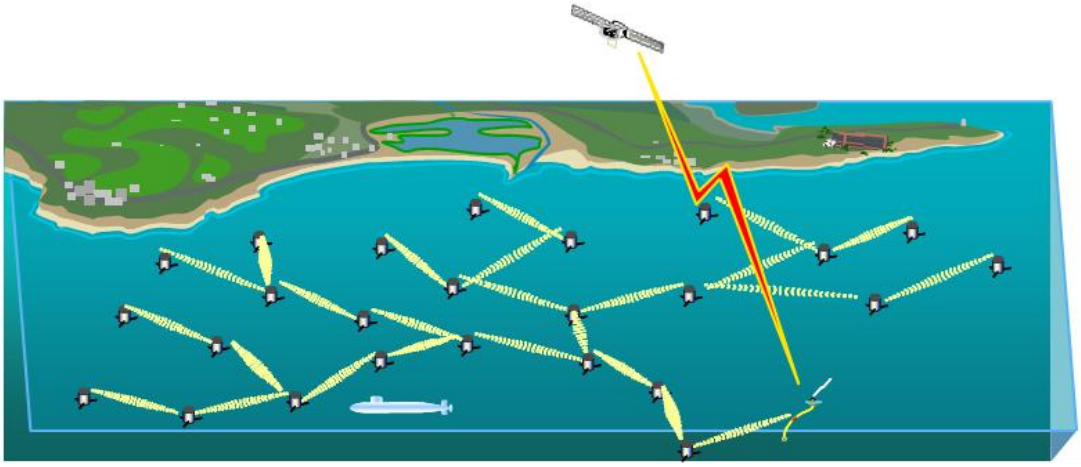

Figure 3. Example Seaweb system [From 6]

C. DEEP OCEAN CHARACTERISTICS

The deep ocean is characterized by persistent features conducive to long-range acoustic communications. Acoustic modem systems, such as Seaweb, could exploit well-known phenomena, such as Reliable Acoustic Path (RAP) and Deep Sound Channel (DSC). Acoustic reciprocity in a static environment implies that acoustic propagation is bidirectional; thus, most acoustic channel properties apply to both transmitted and received signals.

1. Reliable Acoustic Path (RAP)

Sound traveling through the deep ocean can be received through various propagation paths (such as direct path, bottom bounce, surface ducts, etc.) depending on the environment and source/receiver depth. These multipath arrivals are "a common

occurrence in long-range propagation" [7]. While the accumulation of the different arrival paths can cause the received signal to deteriorate, "often one path will be dominant, and the transmission loss corresponding to it will be minimum compared to other possible paths" [7]. One such dominant path is Reliable Acoustic Path (RAP).

The RAP phenomenon occurs when a source is placed at a greater depth than a receiver in the deep sea. Some possible RAPs are shown in Figure 4. As a RAP is "sensitive … neither to near-surface effects nor to the varying losses on reflection that characterize bottom-bounce propagation" [7], it does not suffer scattering losses associated with surface interference or the losses caused by bottom reflection and absorption. A RAP's transmission loss is relatively low compared to other paths.

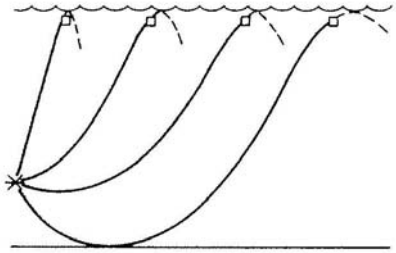

Figure 4. "Reliable" acoustic paths from a deep source to a shallow receiver in the deep sea [From 7]

The RAP characteristics allow for a bottom-mounted or near-bottom device (such as an acoustic modem) to consistently send strong signals to a receiver near the surface. Because of acoustic reciprocity, an acoustic sensor at or near the bottom could also detect objects near the surface. A scenario where this may be useful is with a bottom-mounted sensor detecting a shallow (relative to the bottom of the deep ocean) submarine at predictable RAP distances.

A bottom-mounted sensor uses the RAP to its advantage. A bottom-mounted sensor can monitor a large volume of water within the RAP. It is estimated that the diameter of the surface coverage is approximately 10 times the water depth. As the noise sources outside the RAP volume are strongly attenuated by reflection, absorption, and scattering, the dominant signals are from within the detection range. Also, with the low

ambient noise level at the sea floor, a bottom-mounted device can detect targets or receive data within the RAP volume at high SNR (Signal-to-Noise Ratio).

2. Deep Sound Channel (DSC)

The Deep Sound Channel (or DSC) is caused by the sound speed gradient shift from the surface to the bottom of the ocean. Water temperatures are higher near the surface, which causes sound velocity to increase. As depth increases, temperature decreases, causing sound velocity to decrease. At some minimal velocity, the sound speed gradient goes from negative to positive. At these depths, temperature is isothermal and the effects of increasing hydrostatic pressure becomes the dominant influence on sound speed, causing it to increase with depth [8]. The depth at which there is minimal velocity is called the DSC axis "toward which sound rays are continuously bent by refraction" [8]. The change in gradients creates a duct where the sound rays refract back and forth between axis upper and lower boundaries (see Figure 5) with low transmission loss. Figure 6 shows worldwide DSC axis depths, with a typical axis depth at 1000 m.

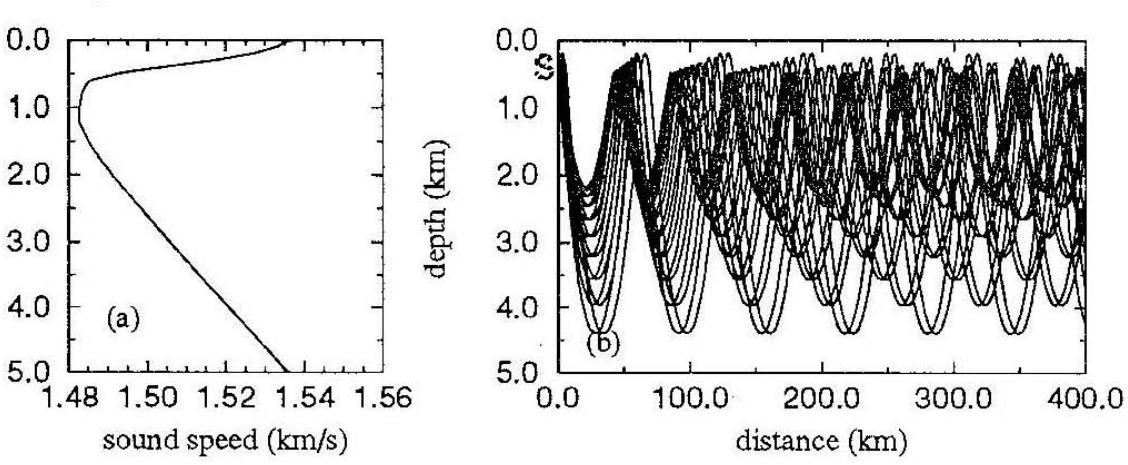

Figure 5. Deep water sound speed profile with ray trace in DSC, source at 500 m [From 9]

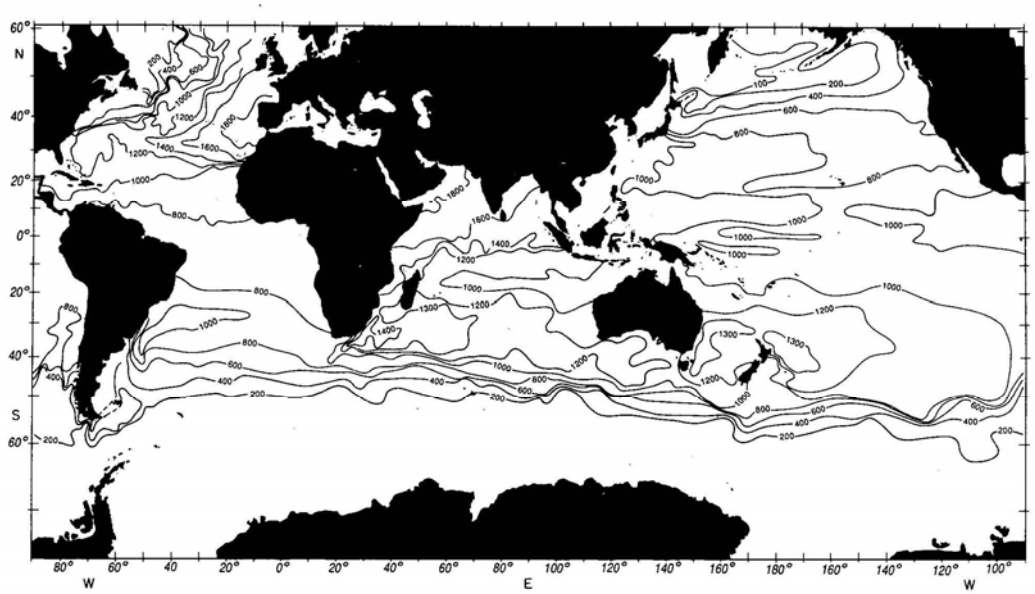

Figure 6. Worldwide DSC axis depths [From 10]

DSCs have been used to provide long-distance undersea communications. After World War II, Ewing and Worzel demonstrated that a small explosive charge could be detonated at the DSC axis and sound transmitted over "long ranges ... made possible by the natural sound channel which exists in the oceans" [11]. They proposed a system of receiver stations that could locate "planes, ships, and life rafts in distress in the open oceans" to "within 1 mile" [11]. At the same time, similar DSC experiments were done by Brehovskikh [12]. More modern uses of DSCs have been for monitoring nuclear tests and for undersea tomography.

DSCs occur where the sound speed profile has a distinctive deep water shape. The Munk canonical equation is "a useful guide to propagation in temperate latitudes" [13]. The Munk equation is given in Equations 1 and 2 [After 13] and is plotted in Figure 7 as a "typical" deep water sound speed profile. Thus,

$$c(z) = 1500.0[1.0 + \varepsilon(e^{-\eta} + \eta - 1)] \tag{1}$$

where

$$\eta = \frac{2(z - 1000)}{1000} \tag{2}$$

and $\varepsilon = 0.00565$ and z = water depth.

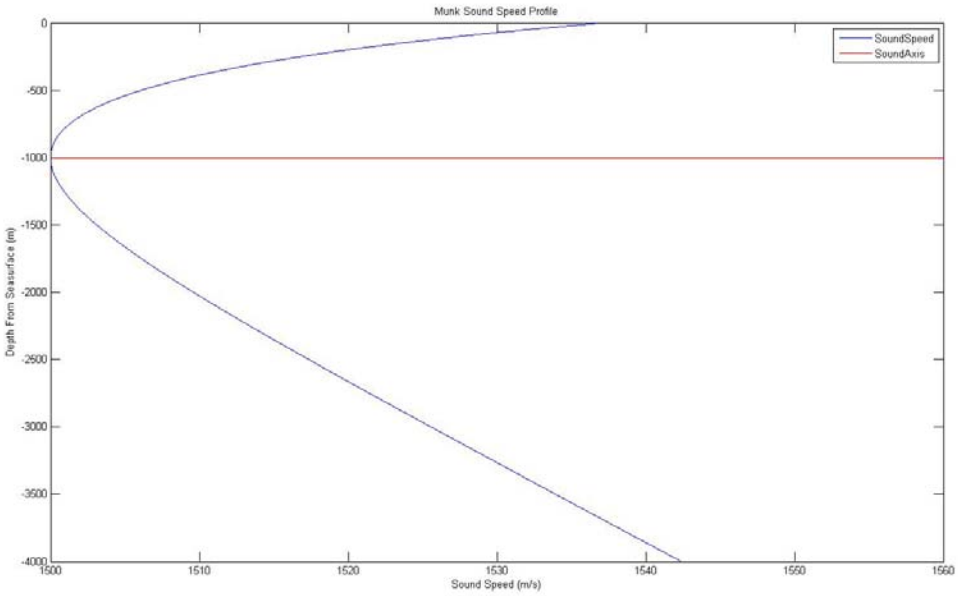

Figure 7. 4000-m Munk sound speed profile

D. DEEP SEAWEB CONCEPT

Acoustic modem networks such as Seaweb could exploit low-transmission loss paths such as Reliable Acoustic Path (RAP) and Deep Sound Channel (DSC). The conceptual system begins with an acoustic sensor at or near the sea floor. A detection of a surface contact or submerged contact is made using RAP. The sensor then transmits via acoustic modem to a sub-surface repeater node. The node is another acoustic modem that can relay the data to an adjacent node using the DSC channel. The data can then either be sent to another node or transmitted upward towards a gateway node such as an USV. The gateway node then relays the data, via satellite or other radio means, to a shore or ship for processing.

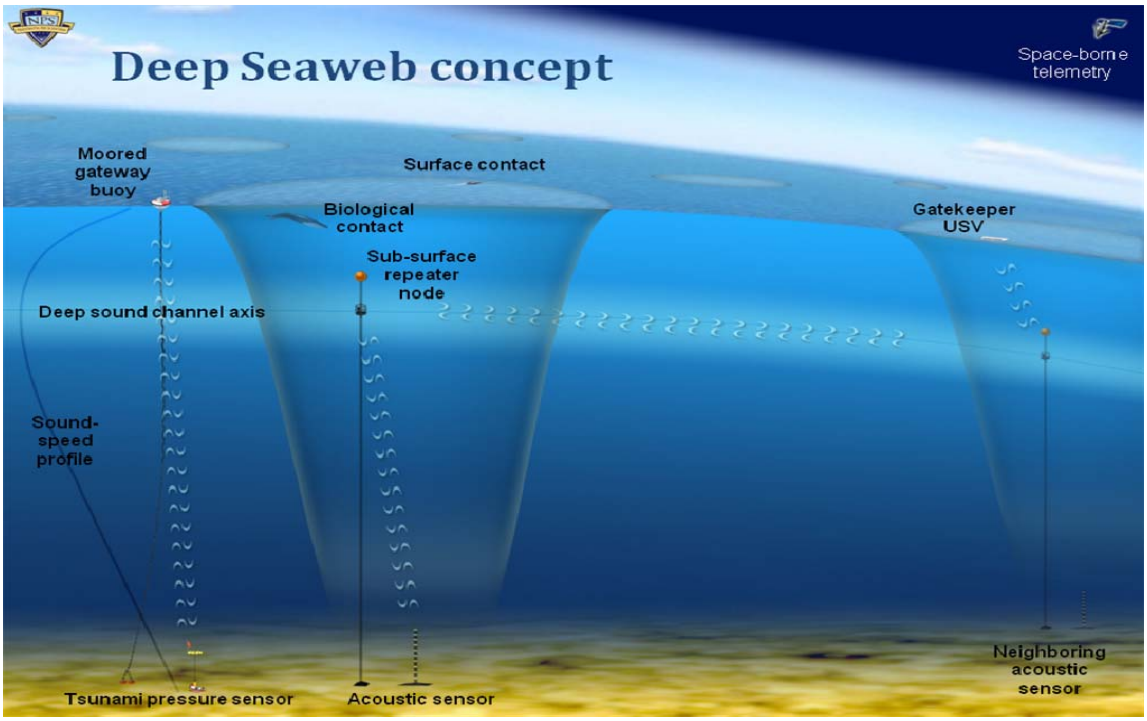

Figure 8. Proposed Deep Seaweb system [6]

A Deep Seaweb system has its advantages. Since DSCs are found worldwide, as shown in Figure 6, the sub-surface nodes can be placed in a variety of locations providing great flexibility to the mission planner. In addition, the use of DSC long-range communication enables nodes to not necessarily be close together but positioned for optimal area coverage.

The characteristics of Deep Seaweb make it appealing for military and civilian applications. In areas such as shipping lanes, sub-surface nodes on the DSC axis (typically 1000 m) are immune to the risk of being hit by a passing ship. For clandestine operations, deep-water placement of nodes and use of low-profile USVs minimizes the number of objects broaching the surface, reducing the possibility of counter-detection. Furthermore, use of the DSC means that the USV does not necessarily need to be near the bottom-mounted sensor. The data transfer can occur with long standoff and be transmitted to the surface at an area that is appropriate.

Deep Seaweb has the potential to be rapidly configurable. In [14], an algorithm was developed for discovery of Seaweb nodes following an ad hoc deployment. The network-layer routes are initialized according to an optimization cost function. If a node is inadvertently removed or damaged, the Seaweb discovery process permits automatic healing of the network routes.

III. ACOUSTIC PROPAGATION MODEL AND LINK MARGIN

A. BELLHOP

Bellhop is a Gaussian beam tracing program [15] used in this thesis to model transmission loss from an acoustic source. Bellhop was chosen for this analysis as "it has proven to be an accurate modeling tool for high-frequency (>1 kHz) transmissions" [15]. The Bellhop program was developed by Porter and Bucker at the Space and Naval Warfare Systems Center in San Diego in 1987 [15].

The AcTUPℓ (Acoustic Toolbox User-interface & Post-processor) program, created by Maggi and Duncan of Curtin University of Technology in Perth, Australia [16], provides the front-end support for the version of Bellhop used in this analysis. The principal environmental inputs into AcTUPℓ include a range-dependent Sound Speed Profile (SSP), water depth (z) and water density (ρ_1). The program allows for the consistency of the sea floor (such as sound speed c_2, attenuation coefficient, and density ρ_2) to be added to measure the reflection from the bottom. Acoustic system inputs are frequency (f), source depth (z_S) and receiver depths (z_R).

1. Bellhop Validation

To demonstrate the validity of the Bellhop program at frequencies as high as 10 kHz, several cases were tested to compare the Bellhop model with the expected theoretical results. The MATLAB program in Appendix A calculates the transmission loss from a source to a receiver, using an isospeed sound velocity profile. The program calculates the amplitude of pressure (P), with respect to depth and range, to find the transmission loss (TL). The program uses Lloyd's mirror (otherwise known as the method of images) to find the direct path and both surface and bottom interference pressure contributions. These pressures are then combined to calculate total pressure from the source to the receiver. The sea surface and sea floor are assumed to be flat and ρ_1 is assumed to be constant using Kinsler et al.'s value of 1024 kg/m^3 [17]. An example of

the Lloyd's mirror geometry is shown at the surface in Figure 9. The geometry at the sea floor is similar, except in the opposite direction. Included in Table 1 are the symbols used in the supporting equations below.

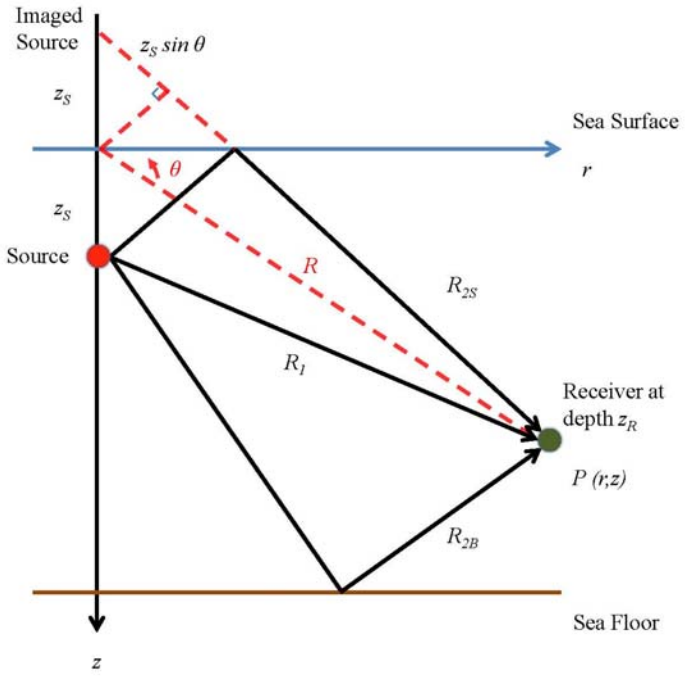

Figure 9. Lloyd's mirror geometry [After 18]

Table 1. Lloyd's mirror symbols

Symbol	Equation Definitions and Units
z_R	Receiver depth (m)
z_S	Source depth (m)
z	Bottom depth (m)
r	Horizontal range (m)
R	Range from surface (at r = 0) to receiver (m)
R_1	Direct path distance from source to receiver (m)
R_{2S}	Surface reflected distance from source to receiver (m)

R_{2B}	Bottom reflected distance from source to receiver (m)
θ	Angle between R and r (rad)
f	Frequency (kHz)
ω	Frequency (rad/s)
λ	Wavelength (m)
c_1	Sound speed in seawater (m/s)
c_2	Sound speed in sea floor (m/s)
ρ_1	Seawater density (1024 kg/m^3)
ρ_2	Sea floor density (kg/m^3)
γ_1	Intermediate variable used to calculate R_R (m^3/kg)
γ_2	Intermediate variable used to calculate R_R (m^3/kg)
B	Intermediate variable used to calculate R_R (m^{-1})
θ_S	Source angle relative to horizontal used to calculate φ (rad)
φ	Angle of reflection relative to ground (rad)
ψ	Complementary angle of φ (rad)
R_R	Bottom reflection coefficient (1)
k	Wave number (m^{-1})
α	Attenuation coefficient (dB/km)
$P\ (r,z)$	Pressure as a function of range and depth (μPa)
P_{ref}	Reference pressure for water (1 μPa)
TL	Transmission loss (dB)

To find the pressure at a given range and depth caused by direct path and surface interference, first the travel distances R_1 and R_{2S} are found over range r using Equations 3 and 4 [After 18]:

$$R_1 = \sqrt{r^2 + (z_R - z_S)^2} \tag{3}$$

$$R_{2S} = \sqrt{r^2 + (z_R + z_S)^2} \tag{4}$$

Secondly, to account for the attenuation of sound as it travels through seawater, the frequency-dependent attenuation coefficient α is estimated, using Equation 5 [After 18]. Equation 5 is a derivation of the curve in Figure 10.

$$\alpha \simeq 3.3\times10^{-3} + \frac{0.11 f^2}{1+f^2} + \frac{44 f^2}{4100+f^2} + 3.0\times10^{-4} f^2 \tag{5}$$

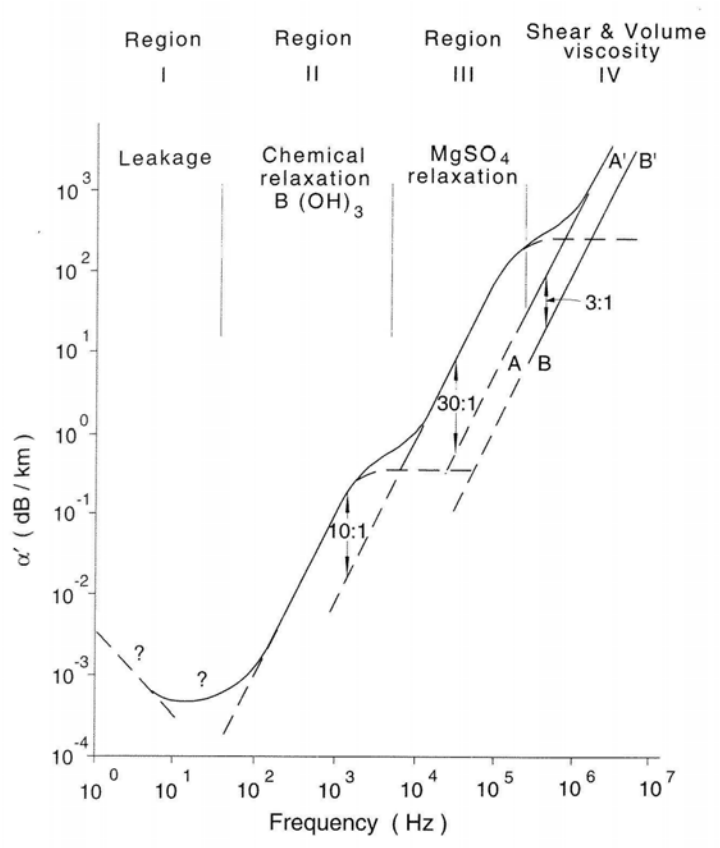

Figure 10. Acoustic attenuation coefficient as a function of frequency [From 18]

Next, the wavelength and, thus, wave number are found using Equations 6 and 7.

$$\lambda = \frac{c_1}{f} \tag{6}$$

$$k = \frac{2\pi}{\lambda} \tag{7}$$

The total pressure amplitude is calculated using Equation 8 [After 18]. The contribution by surface interference is negative compared to that by the direct path. The surface is treated as a pressure release boundary and there is a phase shift, which makes the reflection coefficient R_R = -1 [19].

$$P(r,z) = \frac{e^{ikR_1}e^{-\alpha R_1}}{R_1} + R_R \frac{e^{ikR_{2S}}e^{-\alpha R_{2S}}}{R_{2S}} \tag{8}$$

Lastly, the transmission loss *TL* is calculated by Equation 9.

$$TL = -20\log(\frac{P}{P_{ref}}) \tag{9}$$

For the bottom *TL* calculation, the equations are the similar except that R_{2B} replaces R_{2S} to signify the change in the reference plane for Lloyd's mirror. Also since the sea floor is a fluid-fluid boundary, the reflection coefficient R_R must be found to determine how much of the signal is reflected from the sea floor toward the receiver. The reflection coefficient is found by comparing the density of seawater to that of the bottom, as well as the sound speed change [After 18].

$$R_R = \frac{\rho_2\gamma_1 - \rho_1\gamma_2}{\rho_2\gamma_1 + \rho_1\gamma_2} \tag{10}$$

The variables γ_1 and γ_2 are defined as:

$$\gamma_1 = \frac{\omega}{c_1}\cos(\psi) \tag{11}$$

$$\gamma_2 = B\sqrt{\frac{c_1^{\,2}}{c_2^{\,2}\sin^2(\psi) - 1}} \tag{12}$$

where

$$B = \frac{\omega}{c_1}\sin(\psi) \tag{13}$$

and

$$\psi = \frac{\pi}{2} - \varphi \,. \tag{14}$$

Furthermore, the angle φ is defined as:

$$\varphi = \tan^{-1}\left(\frac{z_S + z_R}{r_1 + r_2}\right) = \tan^{-1}\left(\frac{z_S + z_R}{r}\right). \tag{15}$$

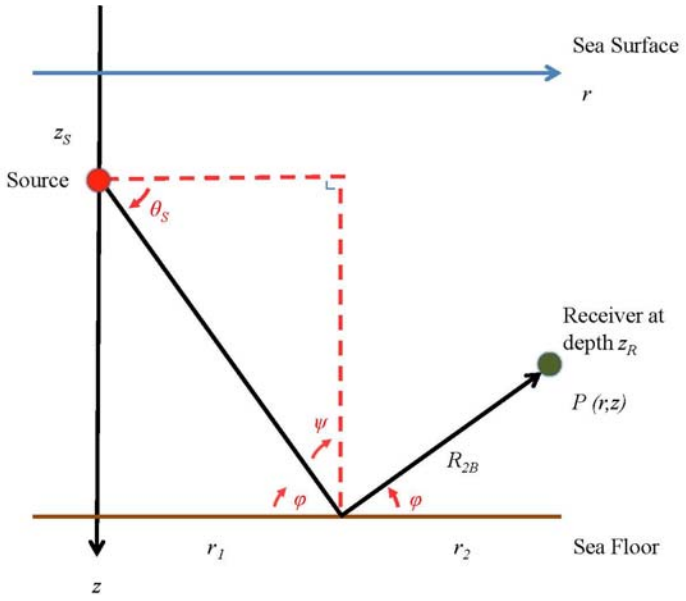

Figure 11. Definition of θ_S, φ, and ψ used to calculate bottom reflection coefficient R_R

With R_R known, Equation 8 is calculated as before and the transmission loss TL is calculated by using Equation 9.

Two examples are used to compare the *TL* calculated by the above equations with that of the Bellhop model. The first example compares the *TL* caused by surface and direct path contributions. A 10-kHz signal emanates from a source z_S = 20 m and is received at z_R = 200 m. The environment consists of an isospeed sound profile with c_1 = 1500 m/s, ρ_1 = 1024 kg/m^3, and water depth z = 5000 m. The two results in Figure 12 are similar.

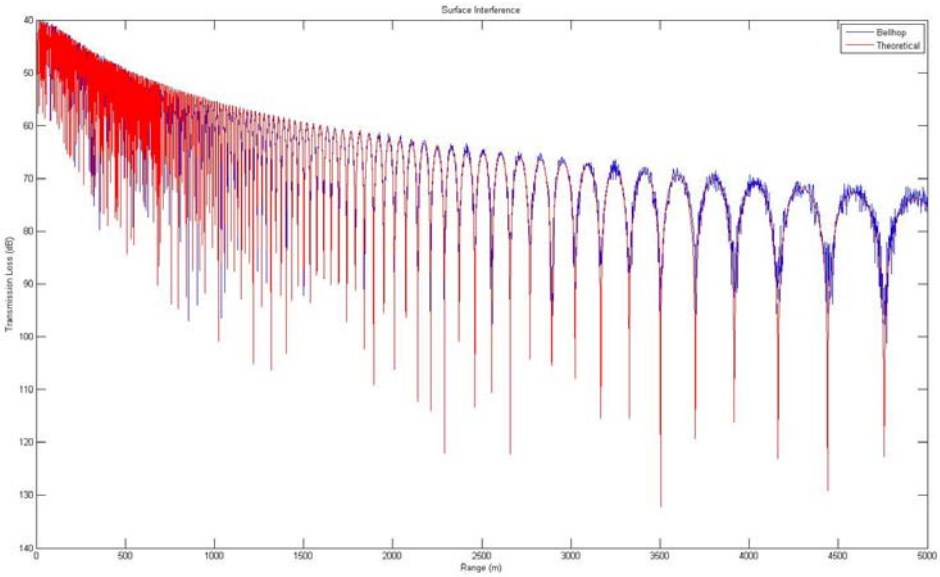

Figure 12. Comparison between direct path and surface *TL* contributions using theoretical and Bellhop values

The second example shows the bottom reflection and direct path contributions. A 10-kHz signal is now projected from a source z_S = 4975m and received at z_R = 4800 m. The water column has an isospeed sound profile where c_1 = 1500 m/s. The sea floor is at a depth of z = 5000 m has properties of c_2 = 1800 m/s and ρ_2 = 1843 kg/m^3. The theoretical and Bellhop *TL* closely track each other in Figure 13.

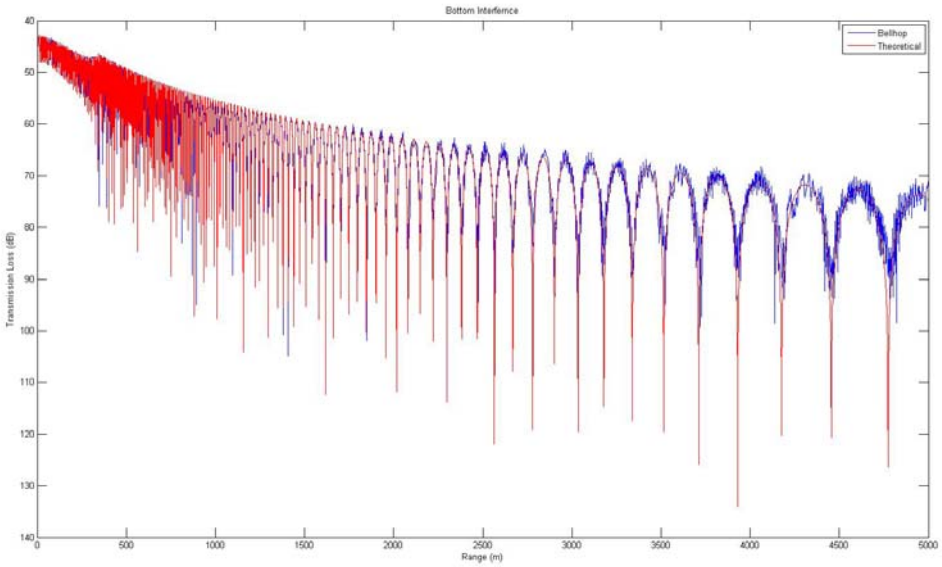

Figure 13. Comparison between direct path and bottom *TL* contributions using theoretical and Bellhop values

The Bellhop program *TL* values match the theoretical values given the same initial conditions. Bellhop is considered validated for the remainder of this study.

B. SONAR EQUATION

The ability of a receiver to detect a signal requires it to be above the environmental and equipment noise that can limit detection. The passive sonar equation in Equation 16 gauges the ability of a transducer to detect acoustic signals. Rearranging the passive sonar equation [After 7], the required level needed to detect a sound is given by:

$$SNR = SL - NL + DI - TL \tag{16}$$

Table 2. Passive sonar equation symbols

Symbol	Equation Definitions and Units
SNR	Signal to Noise Ratio (dB)
SL	Source level (dB re 1μPa @ 1 m)
NL	Noise level (dB)
DI	Directivity index (dB)
TL	Transmission loss (dB)

Each component of the passive sonar equation contributes positively or negatively to the Signal-to-Noise Ratio (*SNR*). The components are measured in dB, requiring them to be normalized by a reference value. A typical dB calculation is $20\log(\frac{\text{Value}}{\text{Reference Value}})$.

The source level (*SL*) is the radiated pressure level relative to 1 μPa measured at 1 m away from the source. The *SL* is the standard definition for the amount of energy the source puts in the water. Noise Level (*NL*) is the additional received energy caused by outside environmental events (such as wind, shipping, or biological). A higher *NL* makes the signal harder to detect and detracts from *SNR*. Traditionally *NL* is estimated using frequency-dependent Wenz curves which account for sea state, shipping, and wind.

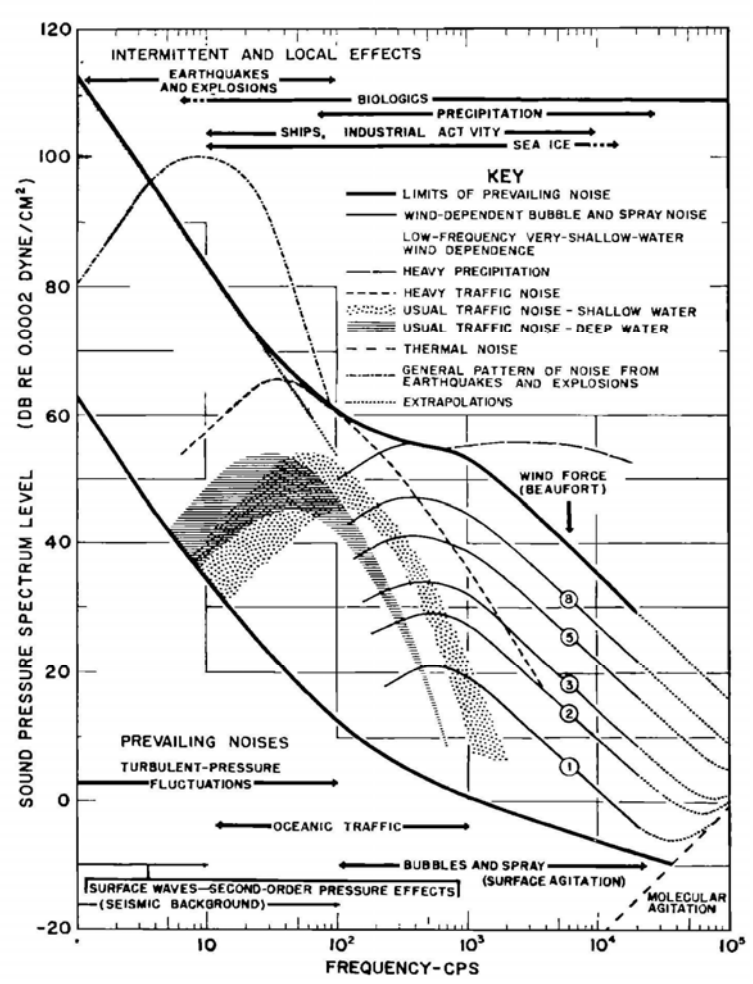

Figure 14. Wenz curves to determine ambient noise level [From 20]

The directivity index (*DI*) is the ability of the transducer to physically or electronically direct its received response in space. An omni-directional transducer can detect a signal in all directions and has $DI = 0$. A directional transducer detects better in a certain bearing and has $DI > 0$ dB.

Lastly the transmission loss (*TL*) is the loss suffered while the signal travels through the medium. The *TL* depends on water column, water depth, and sea floor characteristics. Again because of reciprocity, two identical transducers being used as a source and receiver are interchangeable in terms of *TL*.

For a given sonar system in a given noise environment, as long as the *SNR* exceeds the detection threshold, the signal can be detected. The use of an acoustic model

such as Bellhop can identify sensitivities caused by changes in environmental factors. Using the same initial conditions as for Figure 13, a hypothetical assumption is made that the value of *SL–NL+DI* is 50 dB. For a detection to occur, *TL* needs to be < 50 dB. For *TL* values higher than 50 dB in Figure 15, the losses are too great and detection will not occur.

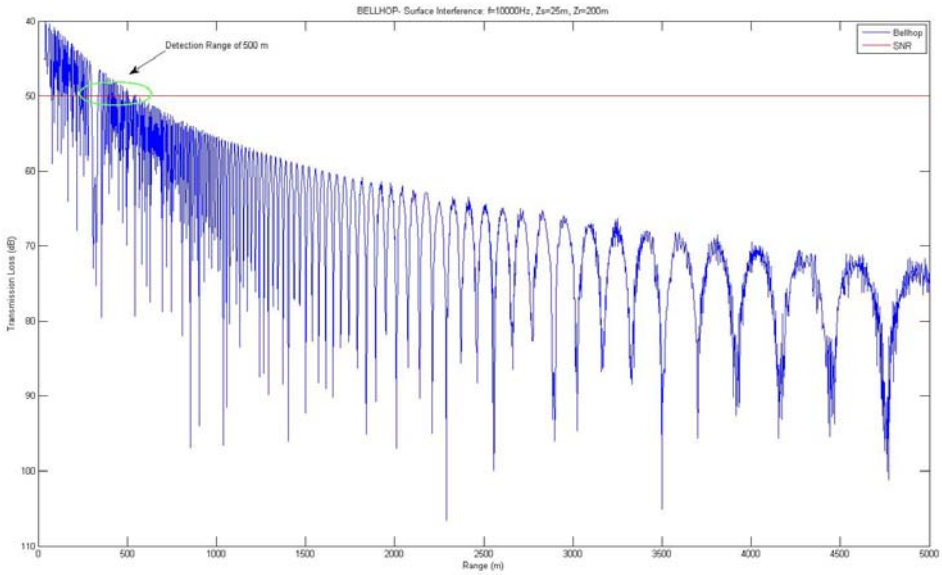

Figure 15. Detection range limit as a function of *TL* for surface interference example

THIS PAGE INTENTIONALLY LEFT BLANK

IV. RELIABLE ACOUSTIC PATH (RAP)

Reliable Acoustic Path (RAP) in the deep ocean can be exploited for sensing and communications. RAP characteristics vary with factors such as transducer placement, water depth and signal frequency. A parametric analysis can reveal how sonar performance in a RAP environment is affected by these factors. The following studies use the property of reciprocity, that is the *TL* experienced from a source to a receiver is the same as if the transducer roles were reversed.

An acoustic modem and sensor apparatus is anchored at the bottom of the ocean, as shown in Figure 16. It is assumed that the acoustic sensor is a transducer baffled such that it provides a hemispherical response. The hemispherical response limits the transducer's ability to detect those signals arriving from 0° to 90° above the horizontal axis.

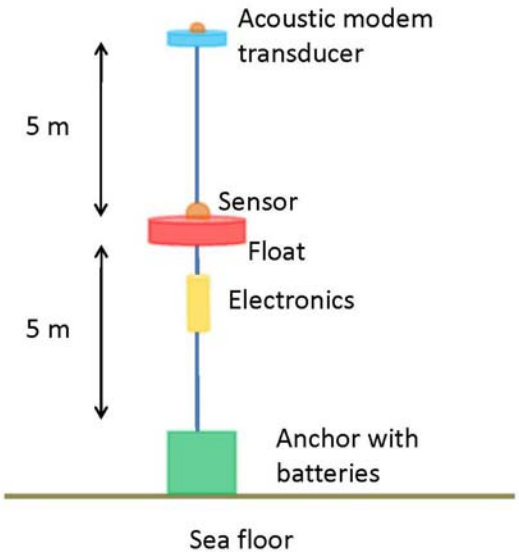

Figure 16. Undersea modem and sensor apparatus for RAP analysis

A. RECIPROCITY

For a 4000-m water column, a Munk profile with the same values as Equation 1 and similar to Figure 7 is considered. The bottom is assumed to be gravel with sound speed c_2 = 1800 m/s and bottom compression attenuation coefficient α_2 = 0.6 dB/λ. Shear losses in the water column and bottom are neglected. A 100-Hz source radiates from a near-surface depth of 30 m, representing a surveillance contact.

Transmission loss, as a function of range and depth, is shown in Figure 16. The brighter areas represent lower transmission loss and the RAP "region" is visible. At approximately 30 km, the RAP ceases to converge with the bottom.

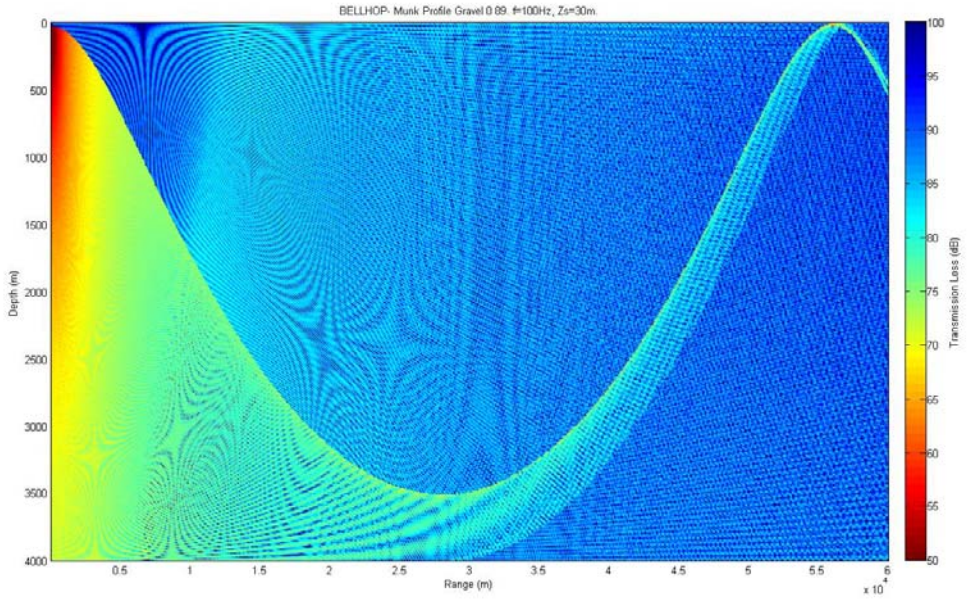

Figure 17. *TL* of a 100-Hz, 30-m source using a 4000-m Munk sound speed profile

The environment is assumed to be static and acoustic reciprocity applies. To demonstrate the property of acoustic reciprocity, a 100-Hz source is placed at a near-bottom depth of 3995 m. Figure 18 shows that the RAP reaches the surface to ranges of 30 km, the same range as in Figure 17. The RAP region seen in Figure 18 exhibits the radial cross-section of the classic "tea cup" surveillance volume for a bottom sensor.

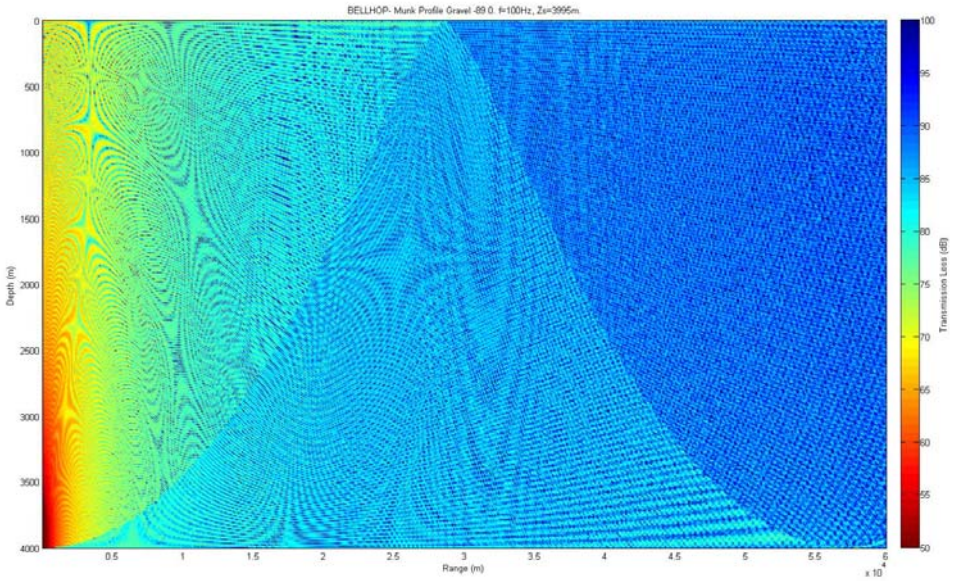

Figure 18. *TL* of a 100-Hz, 3995-m source using a 4000-m Munk sound speed profile

B. DEPENDENCE ON OCEAN DEPTH

With a sensor height of 10 m above the sea floor, the ocean depth is now varied from 500 m to 4000 m and Bellhop *TL* plots are produced for selected ocean depths. The range of maximum signal level (R_{RAP}) is plotted versus ocean depth in Figure 19. The R_{RAP} increases as bottom depth z increases. The plot has three distinct regimes where linear relationships can determine R_{RAP} as a function of bottom depth. From a depth of 0–3.25 km, $R_{RAP} \approx 5.8 * z$. Deeper still from 3.25–3.5 km , $R_{RAP} \approx 6.7 * z$. From 3.5–4 km, $R_{RAP} \approx 7.6 * z$. As the bottom depth gets deeper, the gradient for R_{RAP} gets larger. The diameter of the surveillance area is 12-14 times the bottom depth which validates the rule of thumb stated in Chapter II. For example, a single sensor deployed in 4 km water will have a surveillance area of 2800 km^2!

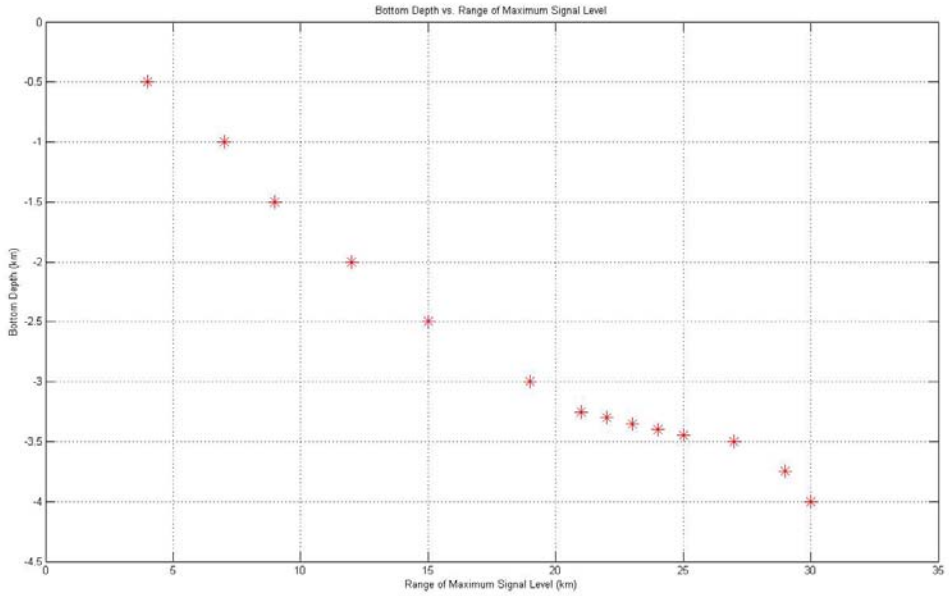

Figure 19. Ocean depth vs. R_{RAP}, 100-Hz, 3995-m source using a 4000-m Munk sound speed profile

C. SENSITIVITY TO MIXED LAYER VARIATIONS

The upper portion of the water column is subject to physical mixing by wind and surface waves. The sound speed in the mixed layer tends to be uniform, with little or no vertical gradient. Using a representative temperate latitude SSP (15.5°N, 179.5°E) from [13], a mixed layer with depths of 50 m and 100 m is introduced in Figures 20 and 21. The remainder of the sound speed profile remains as a 4000-m Munk profile. A mixed layer near the surface of the water column does not appreciably change the detection ranges on the bottom of the ocean, as shown in Figures 22 and 23.

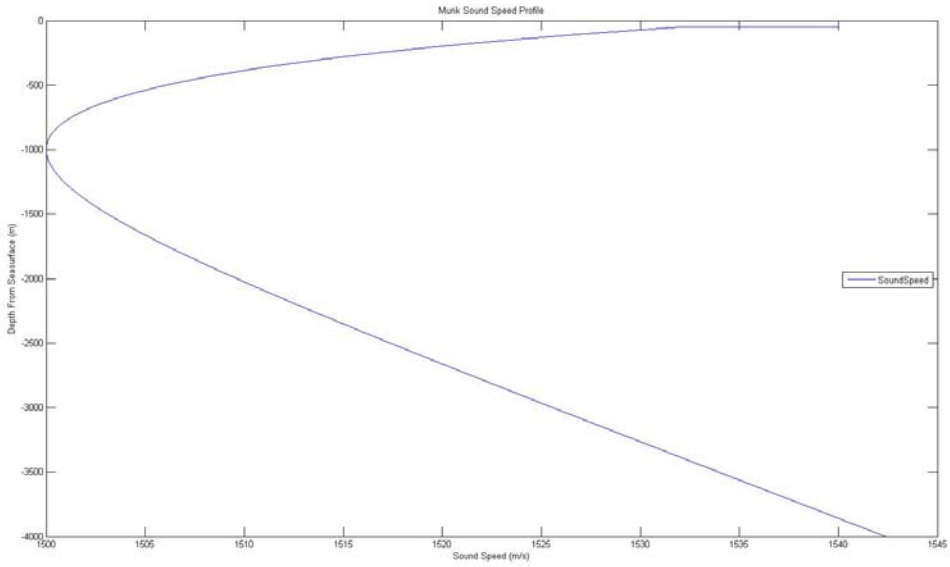

Figure 20. Temperate latitude 4000-m Munk sound speed profile with 50-m mixed layer depth

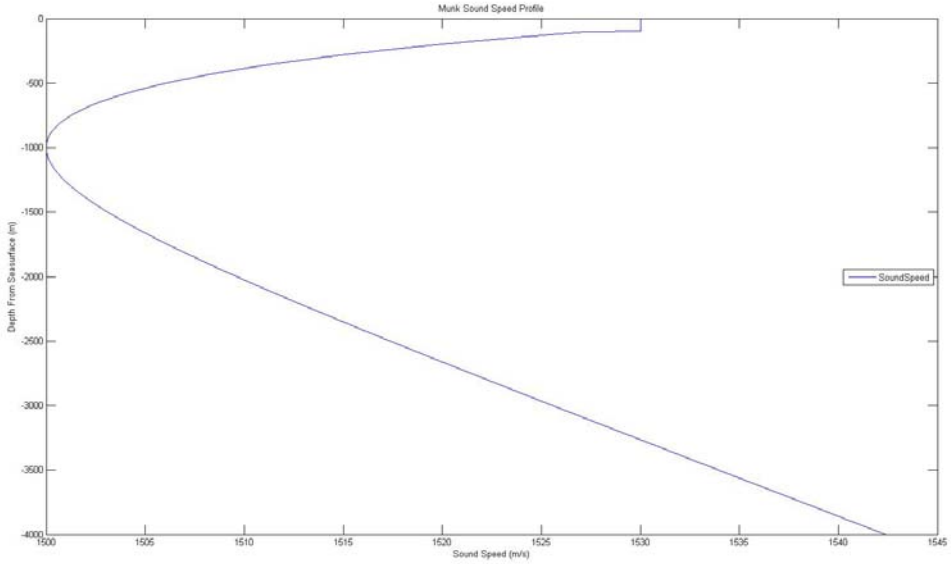

Figure 21. Temperate latitude 4000-m Munk sound speed profile with 100-m mixed layer depth

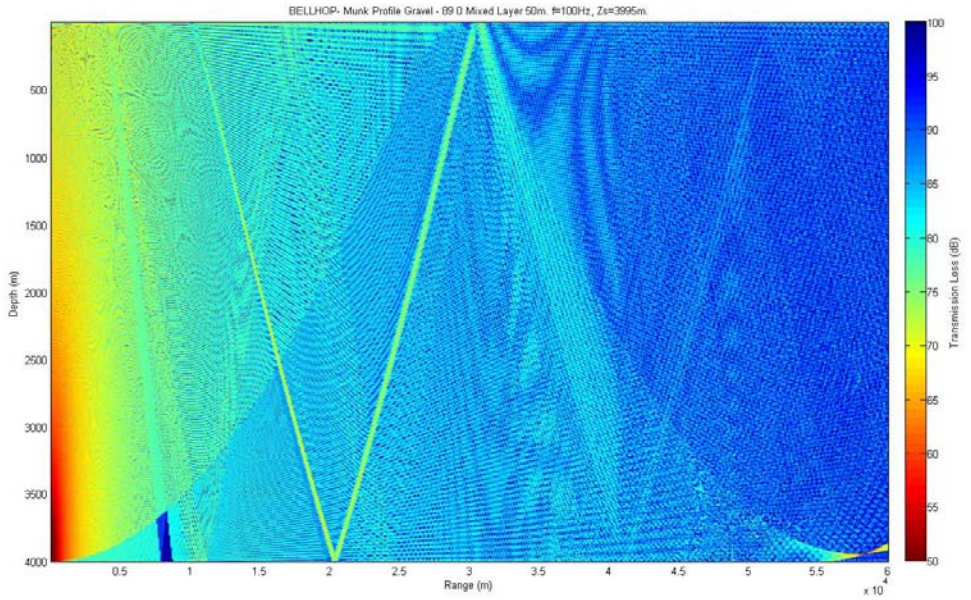

Figure 22. Temperate latitude *TL* of a 100-Hz, 3995-m source in a 4000-m Munk sound speed profile with 50-m mixed layer depth

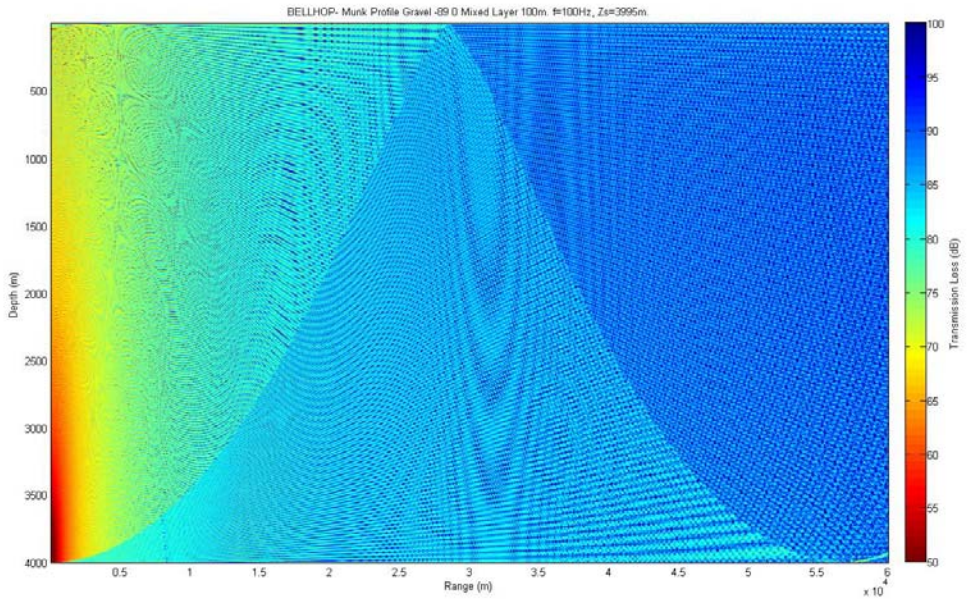

Figure 23. Temperate latitude *TL* of a 100-Hz, 30-m source in a 3995-m Munk sound speed profile with 100-m mixed layer depth

D. FREQUENCY DEPENDENCE

Using a bottom depth of 4000 m and a source depth of 30 m, the frequency is now varied. Figures 24 and 25 show the *TL* for 1 kHz and 10 kHz, respectively. As the frequency increases, so does *TL* due to the frequency-dependent attenuation coefficient α from Equation 5. At 10 kHz, the *TL* is so great that the RAP does not reach the bottom. The significance of this is that acoustic modems that operate in the 9-14 kHz band will have to be placed almost directly beneath a gateway buoy to transmit to the surface.

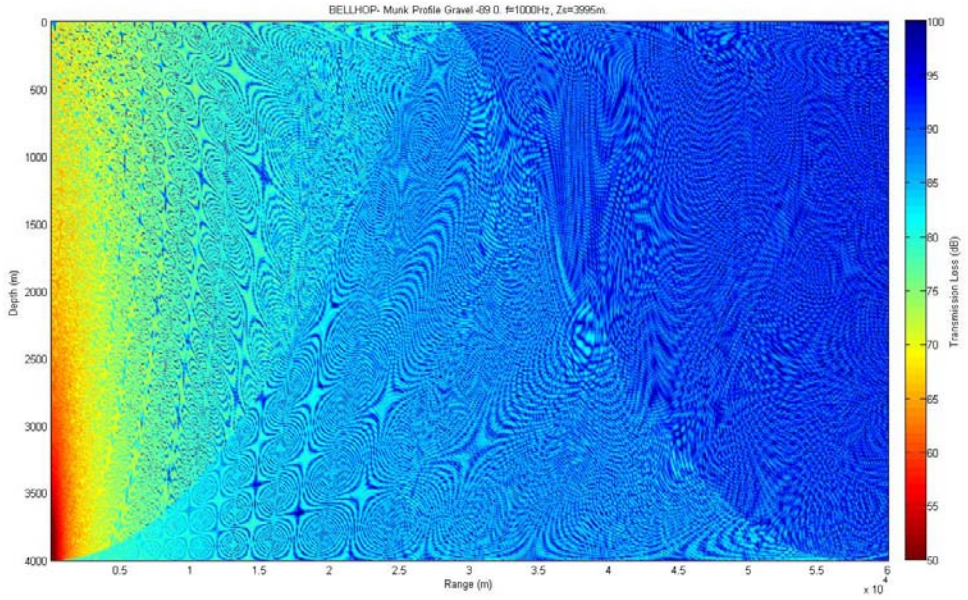

Figure 24. *TL* of a 1-kHz, 3995-m source in a 4000-m Munk sound speed profile

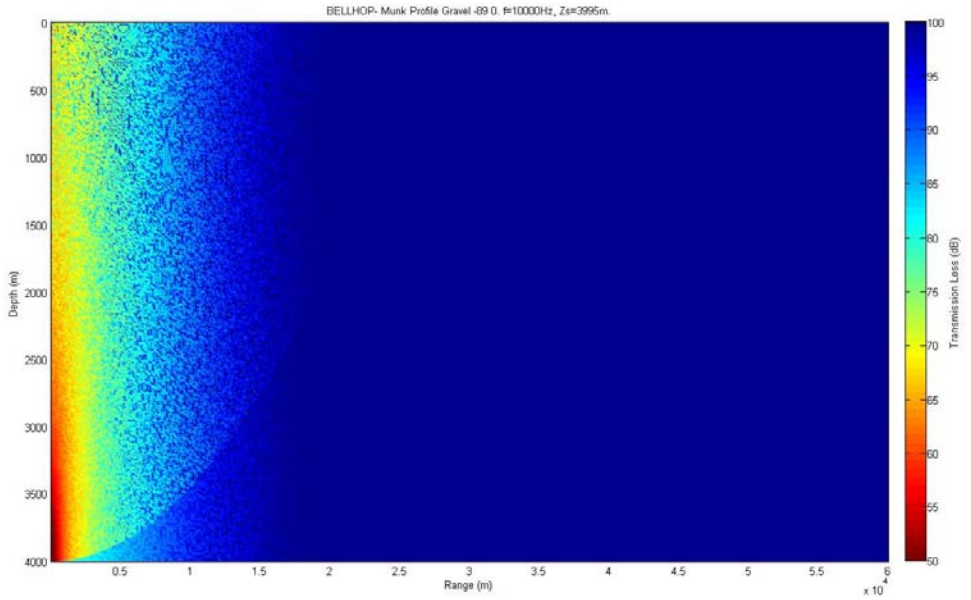

Figure 25. *TL* of a 10-kHz, 3995-m source in a 4000-m Munk sound speed profile

E. LINK BUDGET

Another tool that can be used to gauge the effectiveness of signal transmission through a medium is link budget analysis. A link budget analysis quantifies the ability of the sensor system to detect a signal against a background of noise. Using the passive sonar equation from Equation 16, the *SNR* can be estimated for a sensor's ability to detect the 100-Hz target at depth of 30 m in sea state 3 with normal shipping. From the Wenz curves in Figure 14, the *NL* is estimated to be 43 dB. The *SL* is assumed to be 130 dB (re 1 μPa @ 1 m) and the transducer *DI* is 3 dB. Equation 16 becomes:

$$SNR = 130 - 43 + 3 - TL \tag{17}$$

$$SNR = 90 - TL \tag{18}$$

Detection is likely as long as *TL* is less than 90 dB. Figure 26 shows the detection ranges for the above scenario for a given detection threshold.

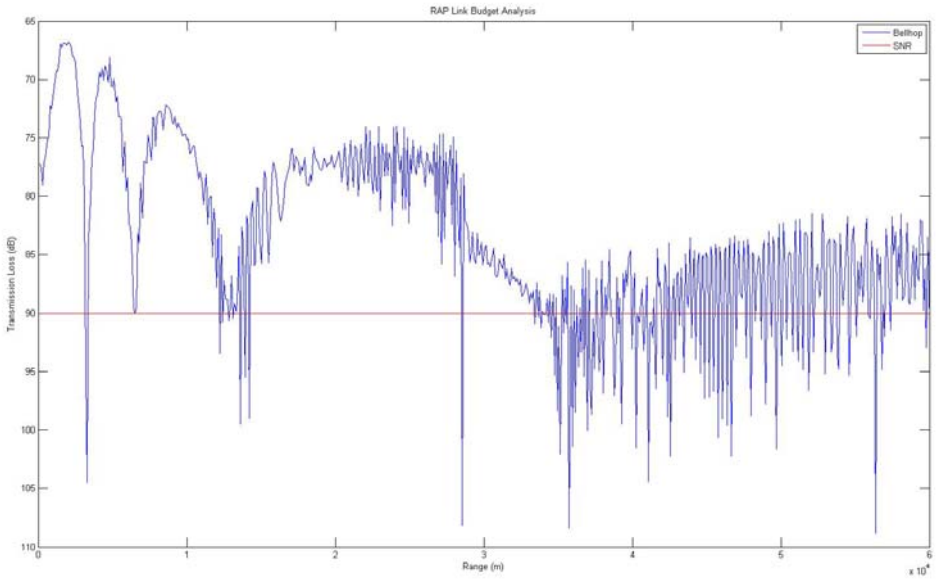

Figure 26. Transmission range of a 100-Hz acoustic modem, 3995-m source and 30-receiver in a 4000-m Munk sound speed profile

F. IMPULSE RESPONSE

The impulse response was extracted from Bellhop using methods discussed in [15]. The impulse response is an indication of the channel time spread produced by multipath propagation from source to receiver. The channel time spread is an important consideration for communications inter-symbol interference (ISI). Some sample paths are shown in Figure 27. Representative impulse responses are shown in Figures 28 and 29.

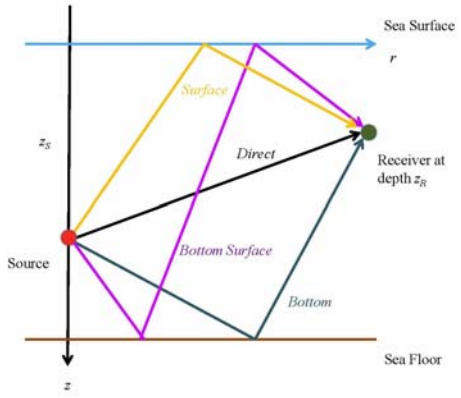

Figure 27. Sample multipath propagation

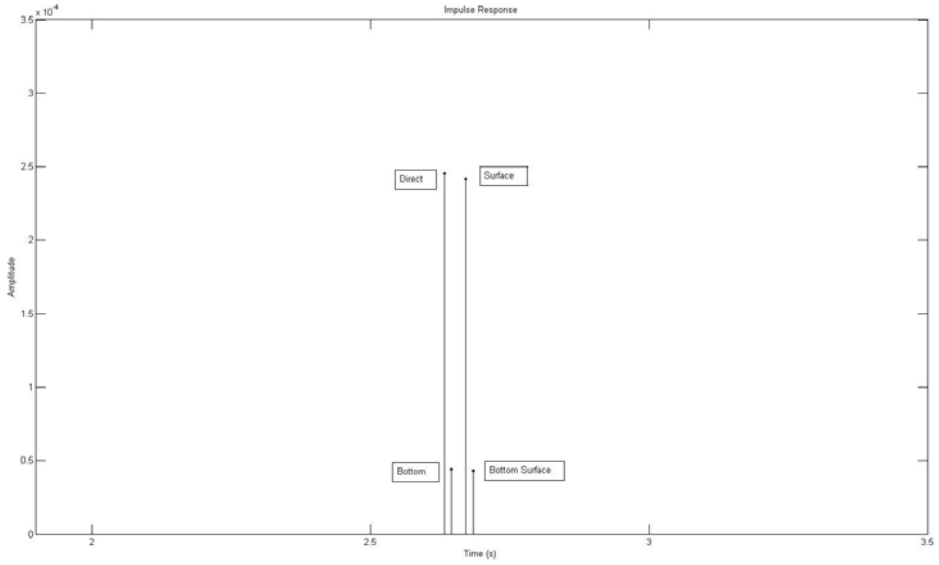

Figure 28. Impulse response for a 7-kHz acoustic modem, 3990-m source and 30-m receiver with launch angles of ±89° in a 4000-m Munk sound speed profile with source-to-receiver range of 500 m

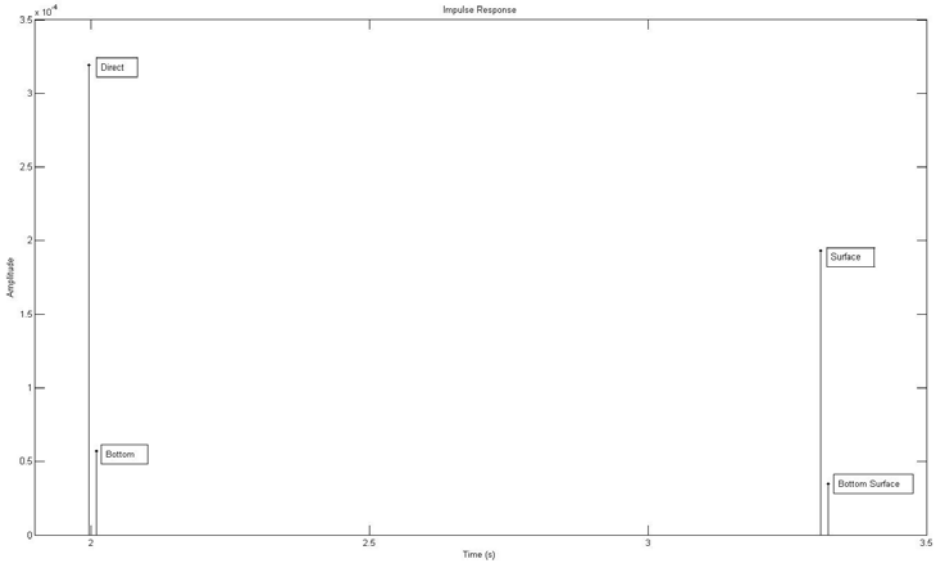

Figure 29. Impulse response for a 7-kHz acoustic modem, 3990-m source and 1000-m receiver with launch angles of ±89° in a 4000-m Munk sound speed profile with source-to-receiver of 500 m

V. DEEP SOUND CHANNEL (DSC)

The system considered in the DSC analysis is an acoustic modem tethered to an anchor on the sea floor as depicted in Figure 30. The water column is characterized by a 4000-m Munk SSP (Figure 7), and the bottom characteristics are the same as for the RAP analysis. The length of the tether is 3000 m optimally placing the acoustic modem placement directly on the sound channel axis at a depth of 1000 m. The standard Seaweb modem operates in the 9-14 kHz band and it is initially assumed for this analysis that the operating frequency is 10 kHz.

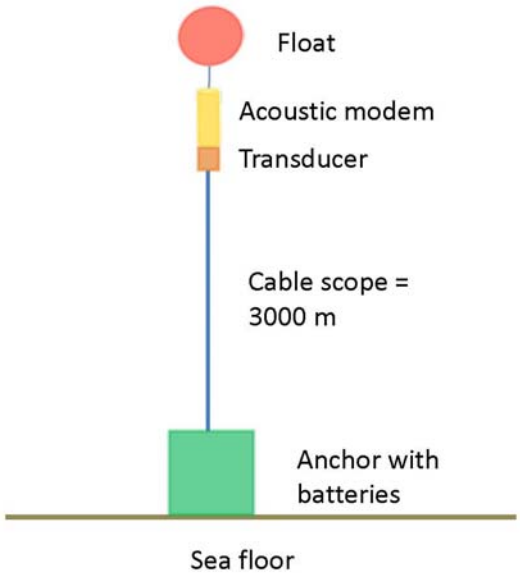

Figure 30. Undersea modem apparatus used for DSC analysis

A. VERTICAL LAUNCH ANGLES

The acoustic modem vertical launch angles dictate the initial trajectory of propagation into the water medium. If the vertical beam pattern is too wide, energy will leak out of the DSC, reach the surface (or bottom) and be wasted. A similar sound speed profile with the source placed at a 1000-m DSC axis is shown in Figure 31.

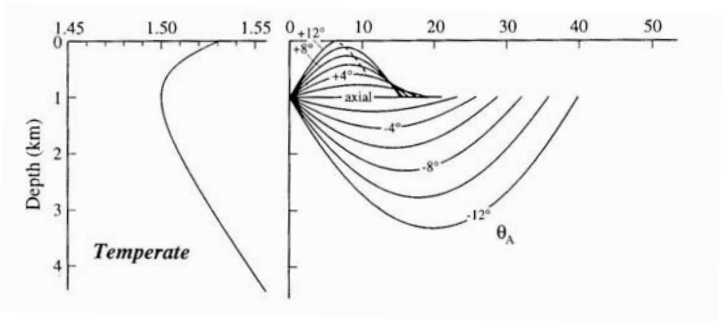

Figure 31. Example of launch angles from source located in DSC axis at a temperate latitude [From 12]

To find the launch angles at which the rays will stay within the DSC, a method developed by Munk [20] is used. The function ϕ is defined as:

$$\phi = \mp\sqrt{(C - C_1) - \varepsilon C_1} \tag{19}$$

where

$$C_1 = \frac{C}{\cos\theta} \tag{20}$$

and C is the depth at the DSC axis and θ is the launch angle.

Equation 20 can be rewritten as

$$\theta = \cos^{-1}(\frac{1}{1+\varepsilon}) \tag{21}$$

Munk defines the sound channel as $\phi = \pm 1$. With $\varepsilon = 0.00565$ as before, θ = ±6°. Figure 32 shows the *TL* for a 10-kHz source at 1000 m with launch angles of ±6°. The maximum range is about 25 km on the axis, where *TL* is 100 dB.

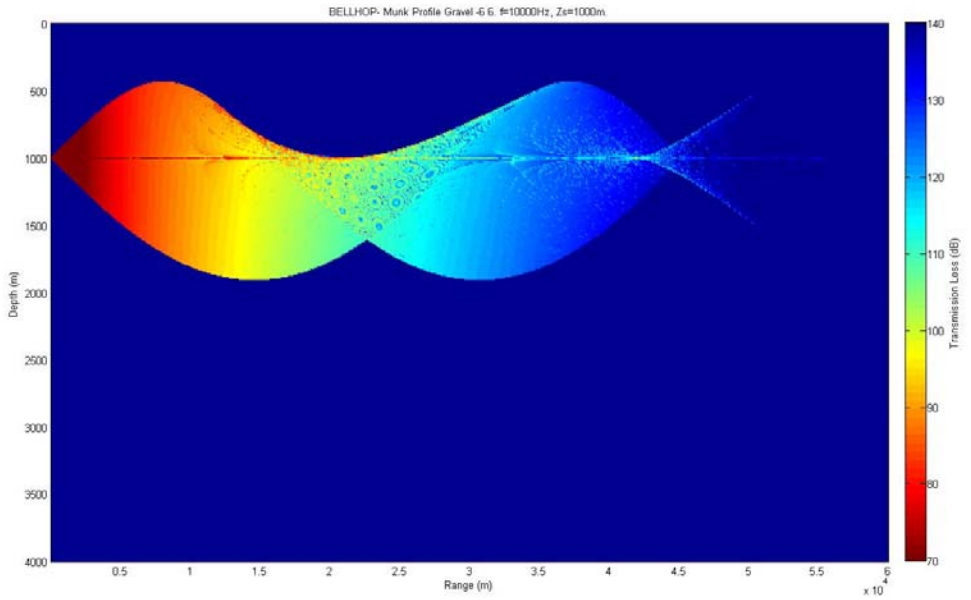

Figure 32. *TL* for a 10-kHz, 1000-m source with launch angles of ±6° in a 4000-m Munk sound speed profile

B. SENSITIVITY TO PLACEMENT AWAY FROM THE DSC AXIS

Outside forces, such as currents, can cause the acoustic modem to deviate from its intended depth on the DSC axis as shown in [22]. In Figures 33 and 34, the modem depth is below the axis by 200 m and 400 m, respectively. When the modem is moved off axis, and maintaining the launch angles at ±6°, the transmitted signal departs the DSC boundaries and the effective range is degraded. At 1200 m and 1400 m depth, the maximum range is about 24 km.

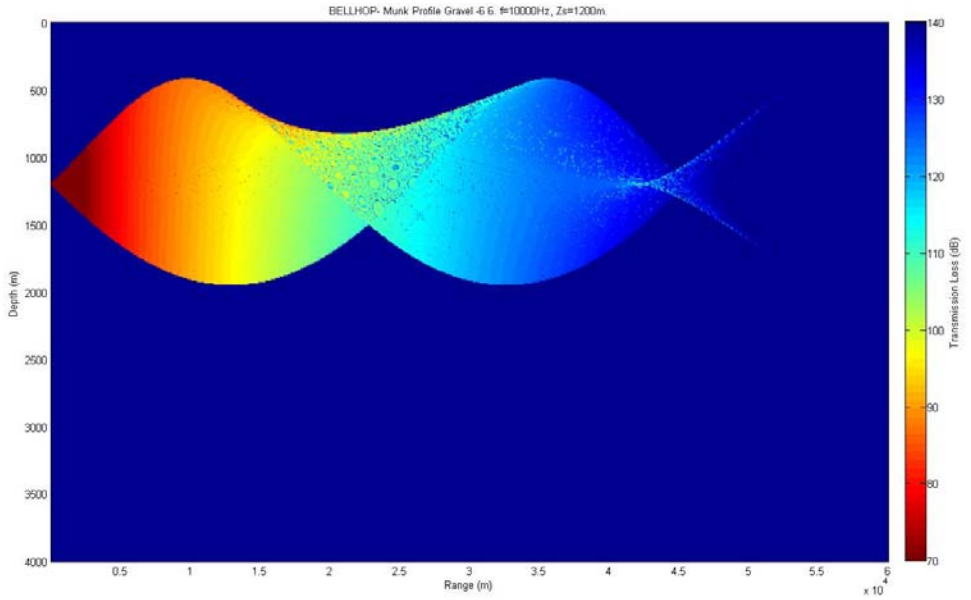

Figure 33. *TL* for a 10-kHz, 1200-m source with launch angles of ±6° in a 4000-m Munk sound speed profile.

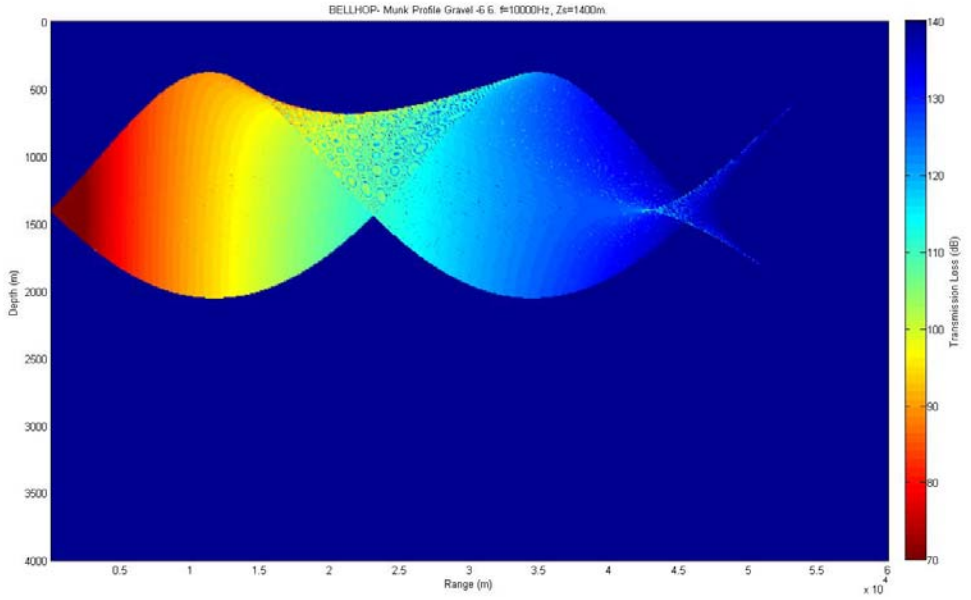

Figure 34. *TL* for a 10-kHz, 1400-m source with launch angles of ±6° in a 4000-m Munk sound speed profile.

A similar analysis with the modem placed at depths of 600 m and 800 m shows the range decreasing to about 21 km. In addition, Figures 35 and 36 predict range regimes wherein there exist shadow zones at the DSC axis when the source is above axis. Placing the source directly on the DSC axis is the optimum location for long-range transmission. Negligible degradation occurs with the source below the axis. Substantial degradation occurs with the source above the axis.

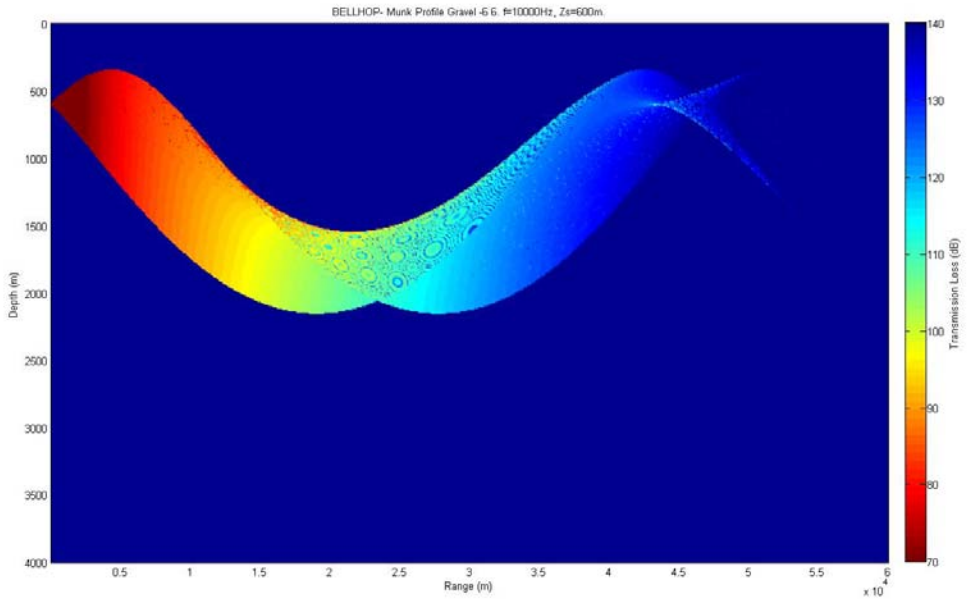

Figure 35. *TL* for a 10-kHz, 600-m source with launch angles of ±6° in a 4000-m Munk sound speed profile.

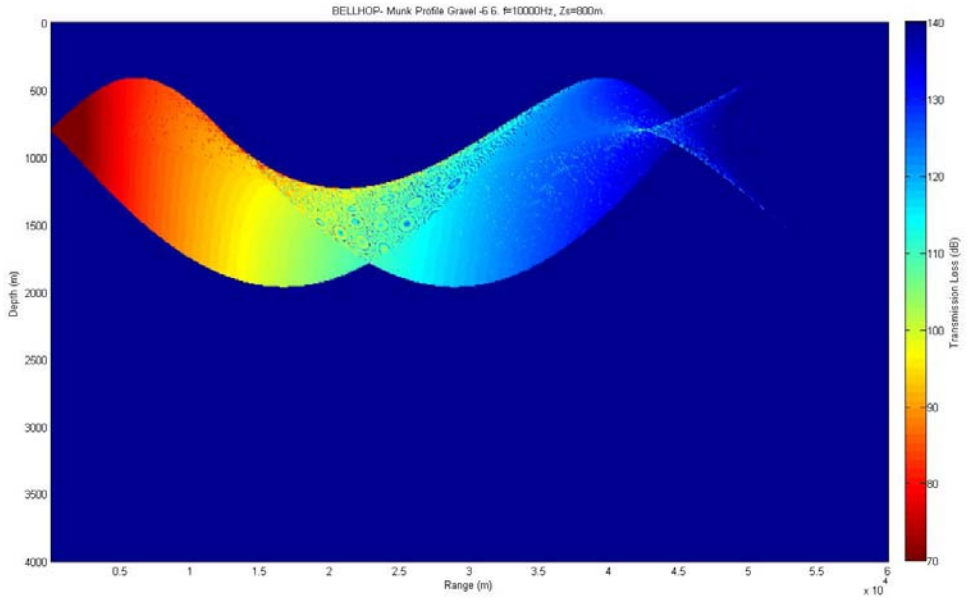

Figure 36. *TL* for a 10-kHz, 800-m source with launch angles of ±6° in a 4000-m Munk sound speed profile.

C. FREQUENCY DEPENDENCE

The acoustic modem is repositioned on the DSC axis for optimum performance. The frequency is now varied to study the effect on *TL*. Figures 37-42 show a progression as frequency increases. The increasing attenuation results in less achievable range.

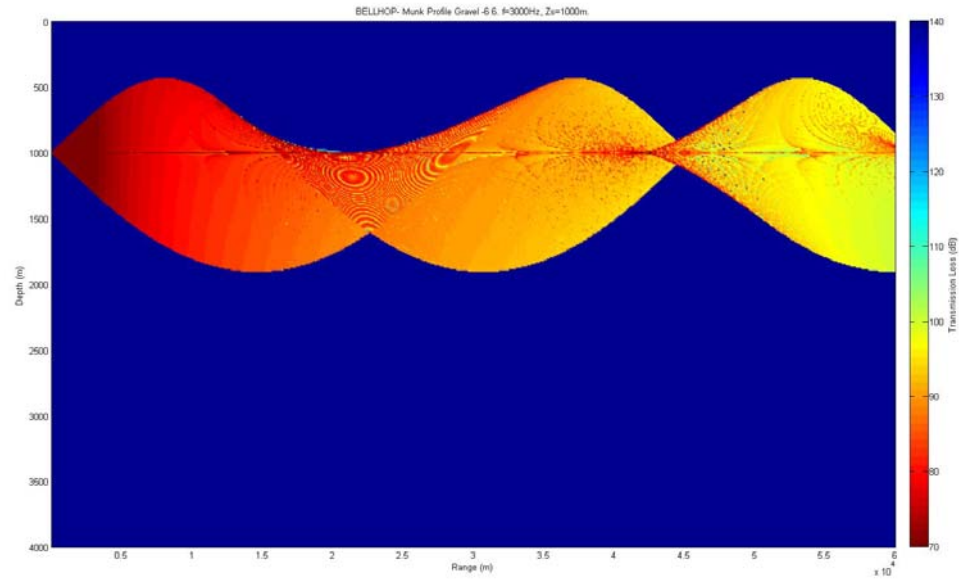

Figure 37. *TL* for a 3-kHz, 1000-m source with launch angles of ±6° in a 4000-m Munk sound speed profile

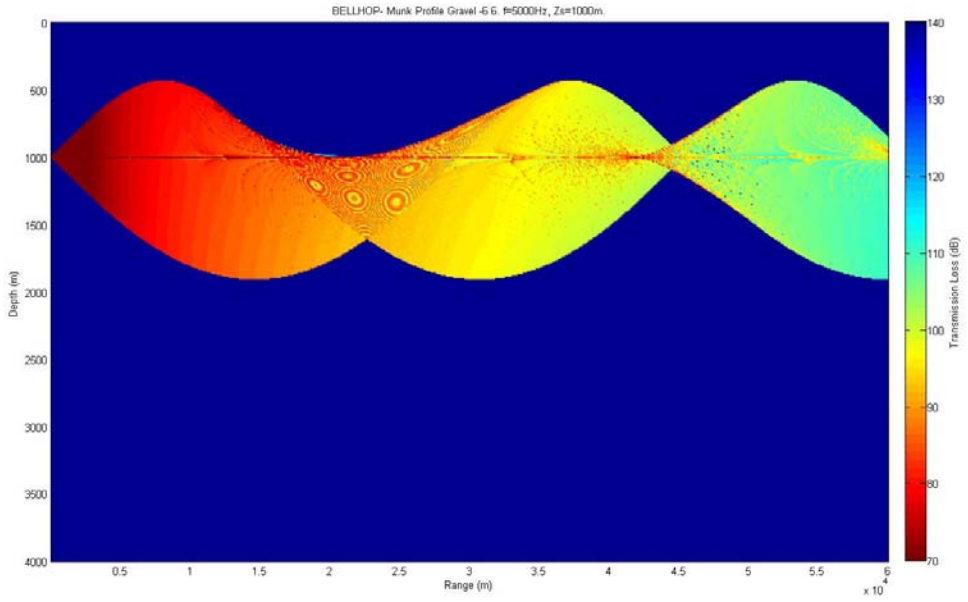

Figure 38. *TL* for a 5-kHz, 1000-m source with launch angles of ±6° in a 4000-m Munk sound speed profile

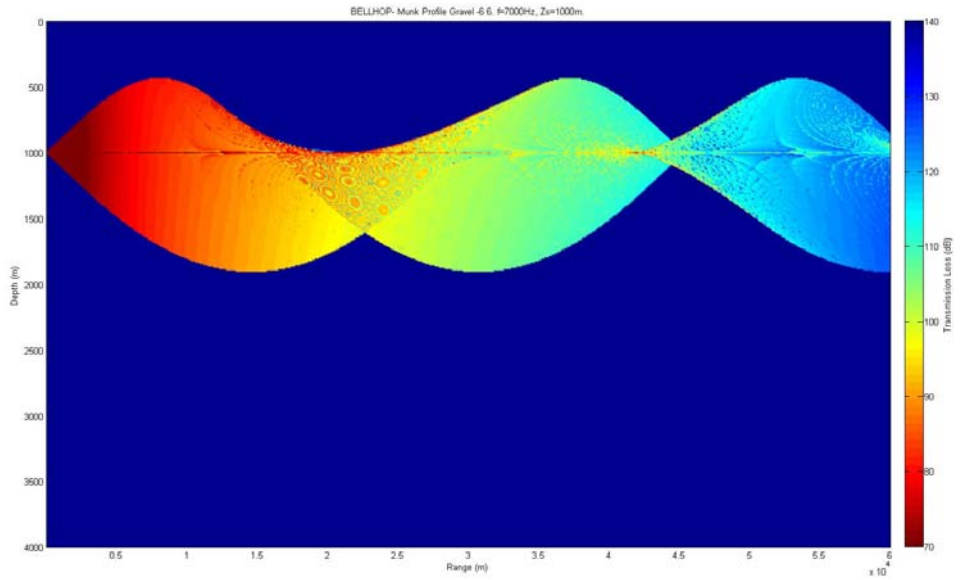

Figure 39. *TL* for a 7-kHz, 1000-m source with launch angles of ±6° in a 4000-m Munk sound speed profile

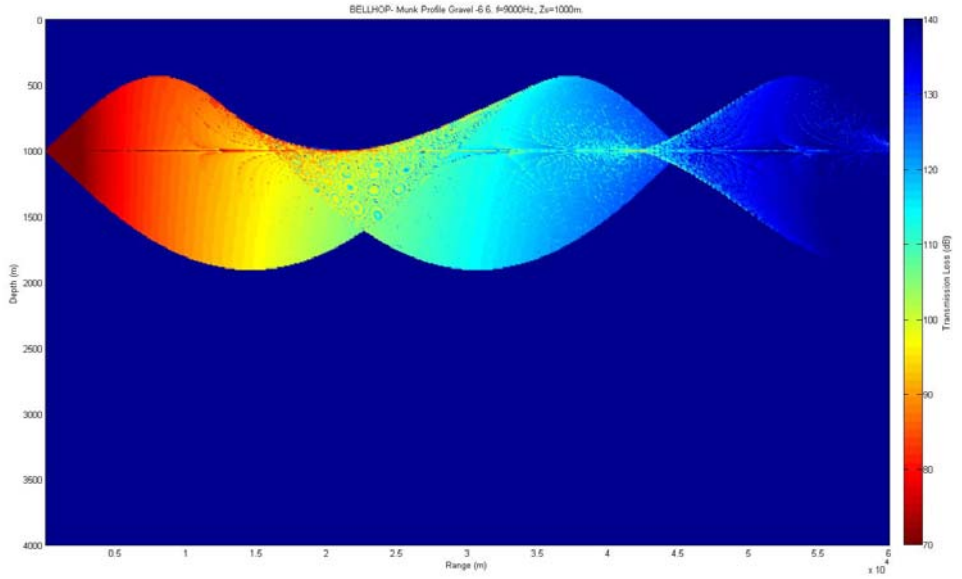

Figure 40. *TL* for a 9-kHz, 1000-m source with launch angles of ±6° in a 4000-m Munk sound speed profile

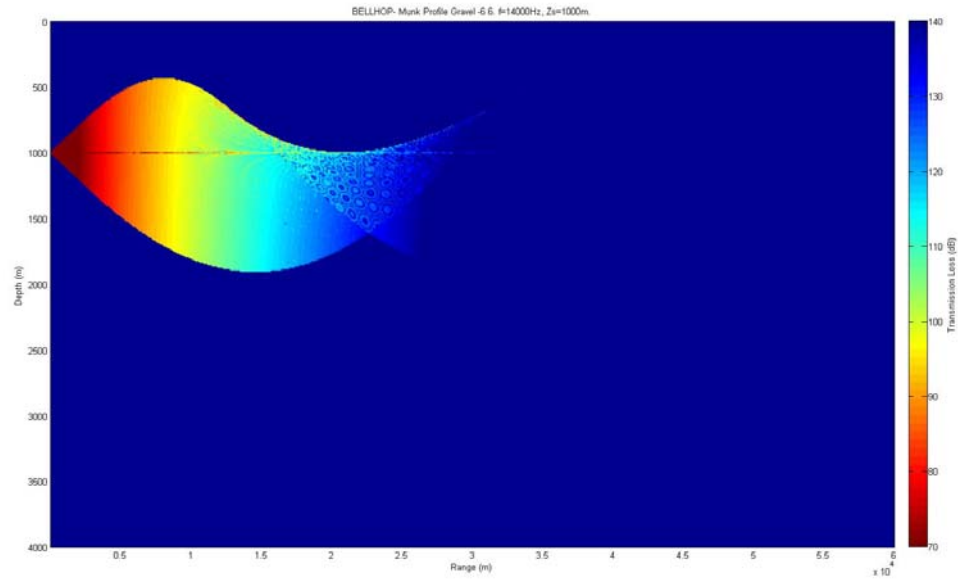

Figure 41. *TL* for a 14-kHz, 1000-m source with launch angles of ±6° in a 4000-m Munk sound speed profile

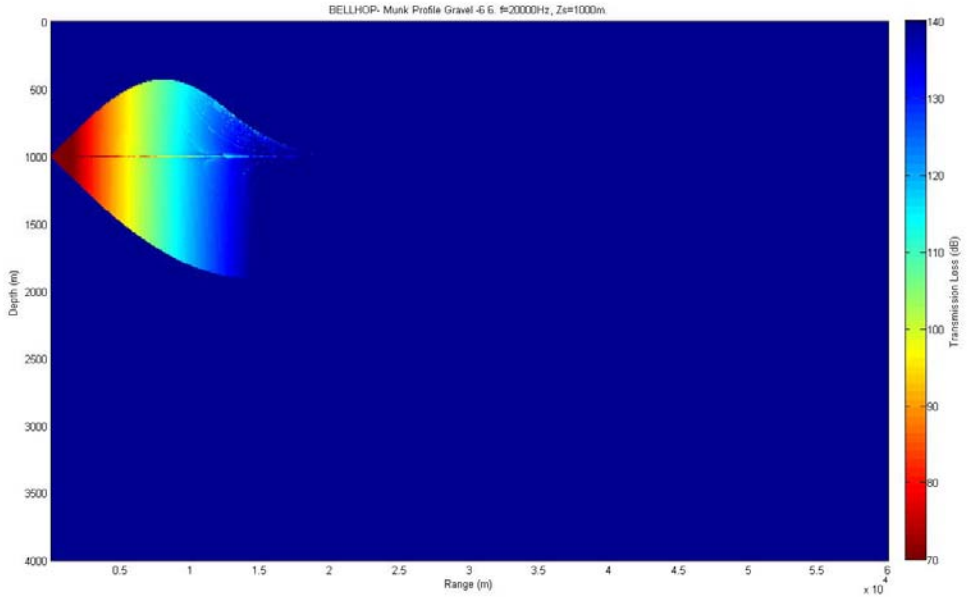

Figure 42. *TL* for a 20-kHz, 1000-m source with launch angles of ±6° in a 4000-m Munk sound speed profile

For select frequencies between 5–13 kHz, the *TL* is plotted versus range. Figure 43 shows that, as frequency increases, the *TL* level increases.

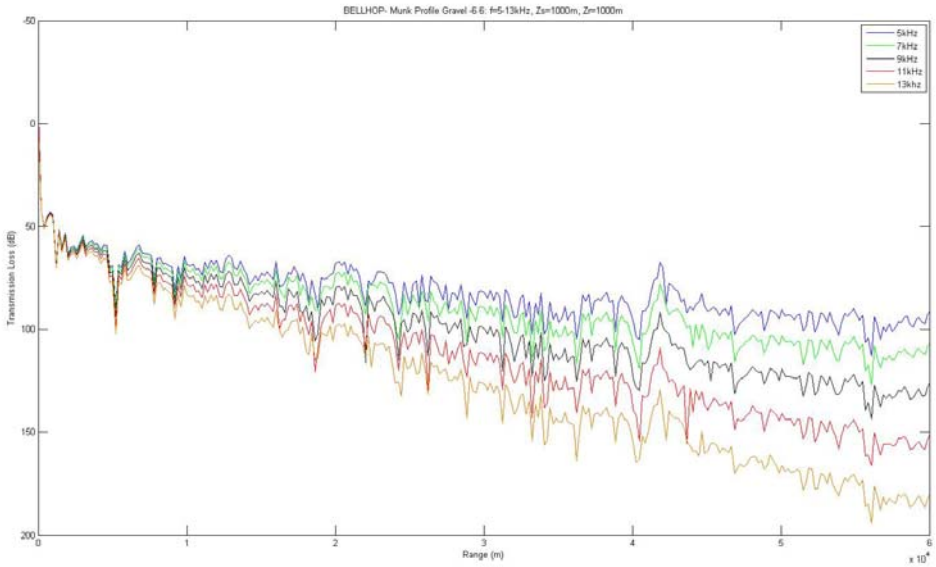

Figure 43. *TL* vs. frequency for a 1000-m source and 1000-receiver with launch angles of ±6° in a 4000-m Munk sound speed profile

D. LINK BUDGET

The link budget analysis using Equation 18 is done for a 7-kHz acoustic modem at a depth of 1000 m. The *SL* is 130 dB with a sea-state 3 *NL* of 18 dB. The *DI* of the modem is 6 dB. The acoustic modem transmits to another modem on the axis.

$$SNR = 130 - 18 + 6 - TL \tag{22}$$

$$SNR = 118 - TL \tag{23}$$

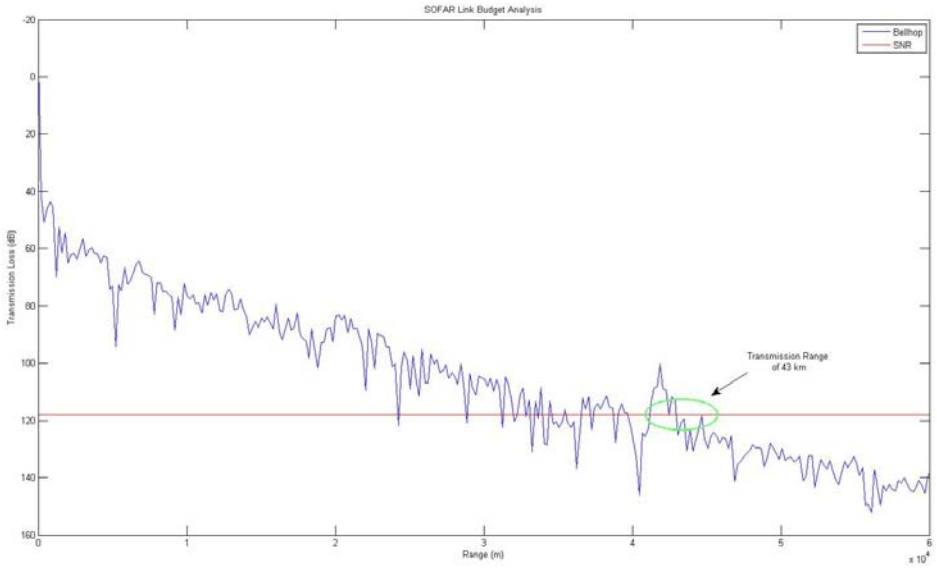

Figure 44. Transmission range of a 7-kHz acoustic modem, 1000-m source and 1000-receiver with launch angles of ±6° in a 4000-m Munk sound speed profile

E. IMPULSE RESPONSE

The modeled impulse response for a 7-kHz acoustic modem at the DSC axis is given in Figure 45.

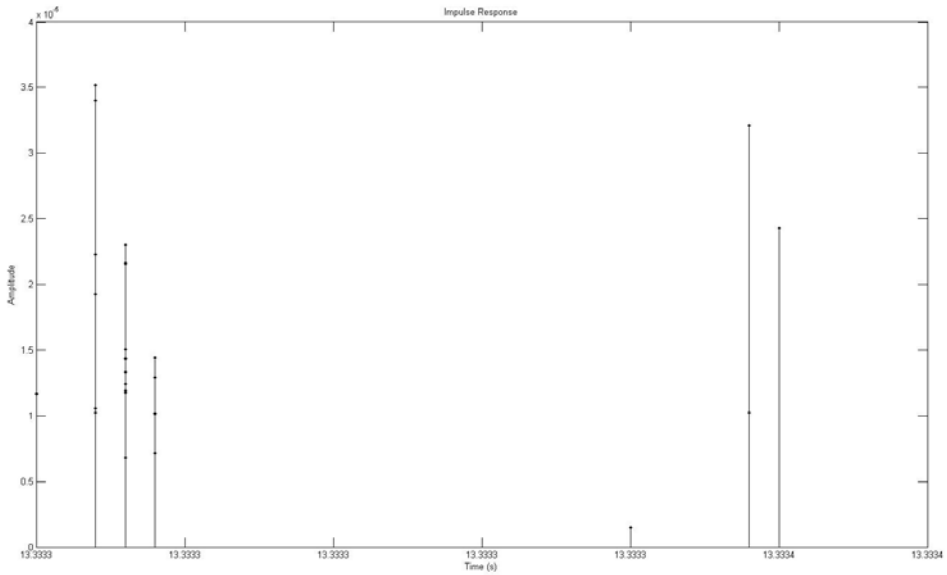

Figure 45. Impulse response for a 7-kHz acoustic modem, 1000-m source and 1000-m receiver with launch angles of ±10° in a 4000-m Munk sound speed profile with source-to-receiver range of 20 km

VI. ACOUSTIC UPLINK TO SURFACE GATEWAY NODE

The final link of the Deep Seaweb network is the communications from the subsea network to a surface gateway node, such as a USV or moored buoy. The link could come either from the bottom-mounted sensor or from a network node placed in the DSC. Figures 24 and 25 show the frequency variations of *TL* from a deep source to a shallow receiver. A higher-frequency (10 kHz) modem at the DSC axis would require the gateway node to be nearly overhead, a lower-frequency modem allows for RAP usage with much greater area coverage. Figures 46-49 show that, as the frequency is reduced, the RAP begins to reveal itself. At 7 kHz, the RAP seems fully formed. In conjunction with lowering the frequency, increasing the upward *DI* of the modem can mitigate *TL* effects.

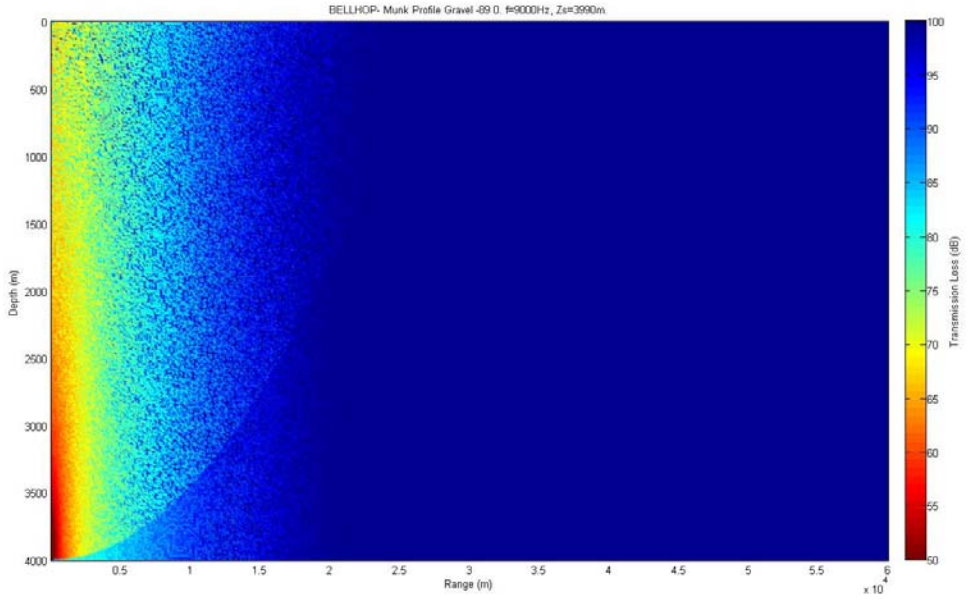

Figure 46. *TL* for a 9-kHz, 3990-m source in a 4000-m Munk sound speed profile

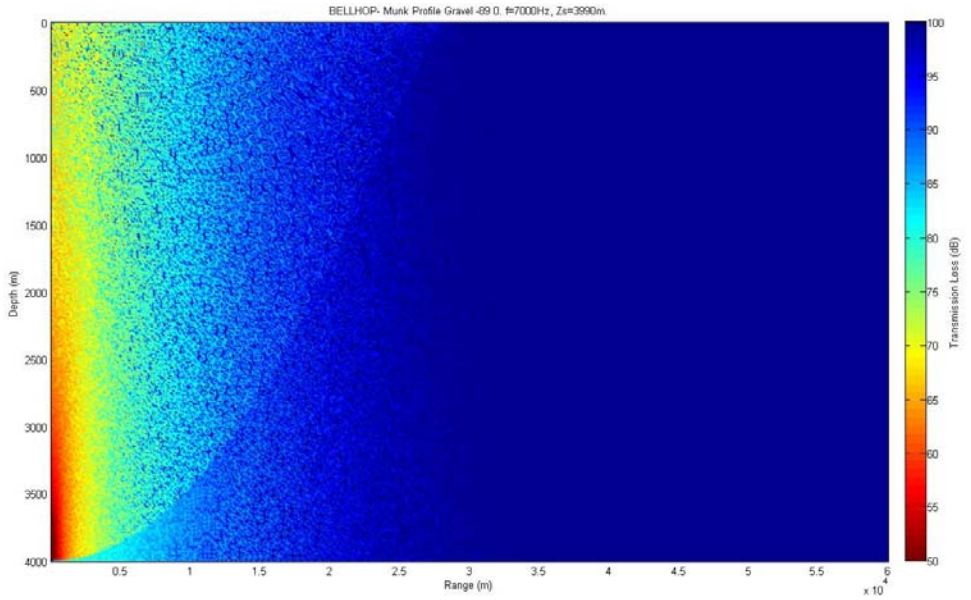

Figure 47. *TL* for a 7-kHz, 3990-m source in a 4000-m Munk sound speed profile

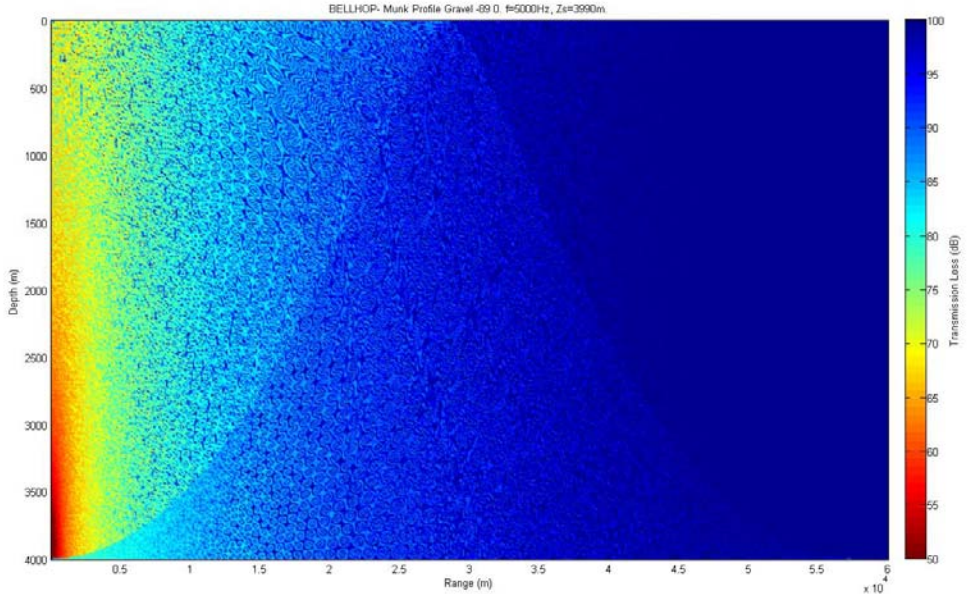

Figure 48. *TL* for a 5-kHz, 3990-m source in a 4000-m Munk sound speed profile

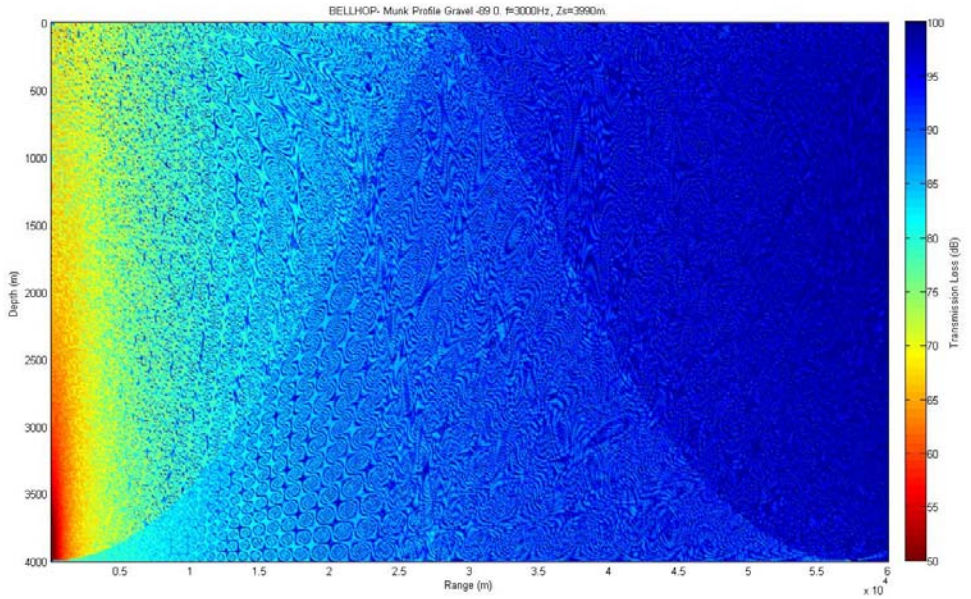

Figure 49. *TL* for a 3-kHz, 3990-m source in a 4000-m Munk sound speed profile

When the source is a modem placed at the DSC axis, the signal has less distance to travel and, thus, suffers less attenuation. Figures 50-53 show that as frequency increases, so does *TL*. However, with less distance traveled, there is less chance for spreading before a boundary interaction and less effective range. Where the effective range for the bottom-mounted modem is around 25 km, the range for a DSC axis node is around 7 km.

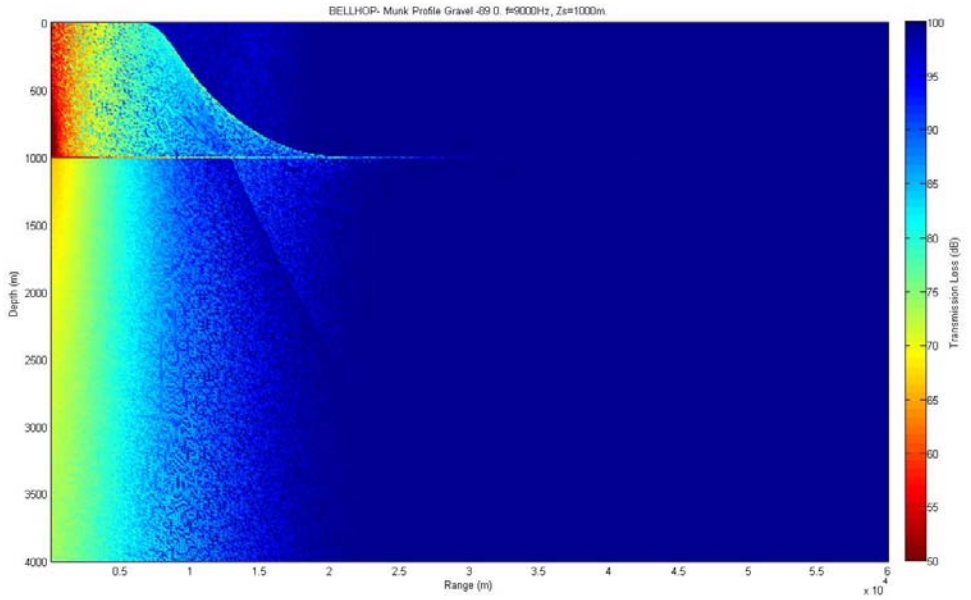

Figure 50. *TL* for a 9-kHz, 1000-m source in a 4000-m Munk sound speed profile

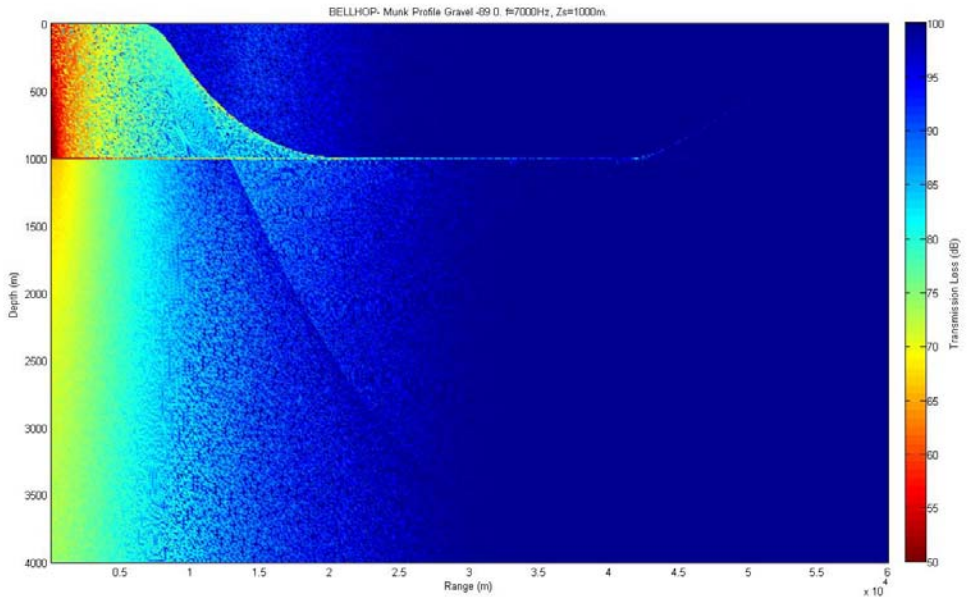

Figure 51. *TL* for a 7-kHz, 1000-m source in a 4000-m Munk sound speed profile

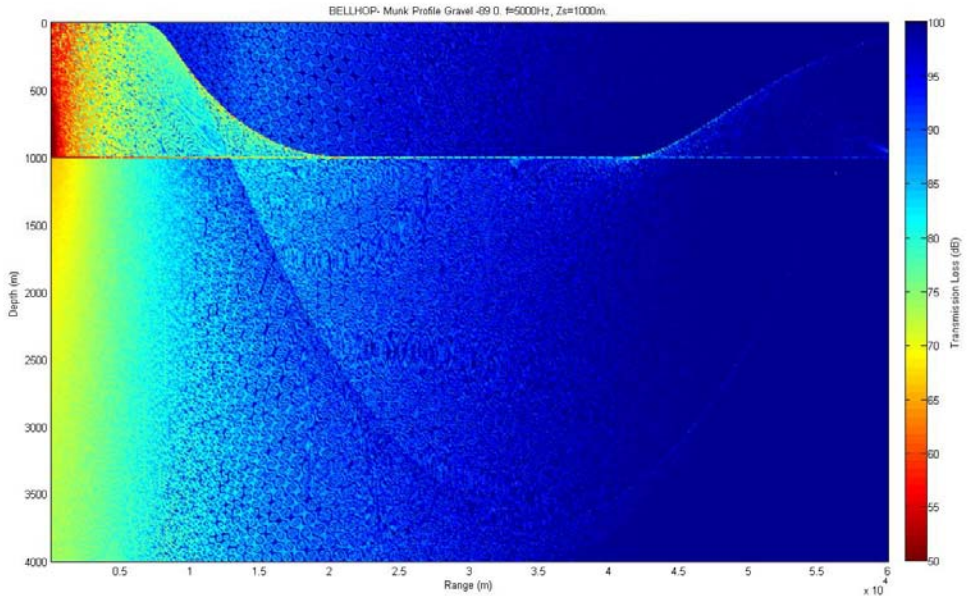

Figure 52. *TL* for a 5-kHz, 1000-m source in a 4000-m Munk sound speed profile

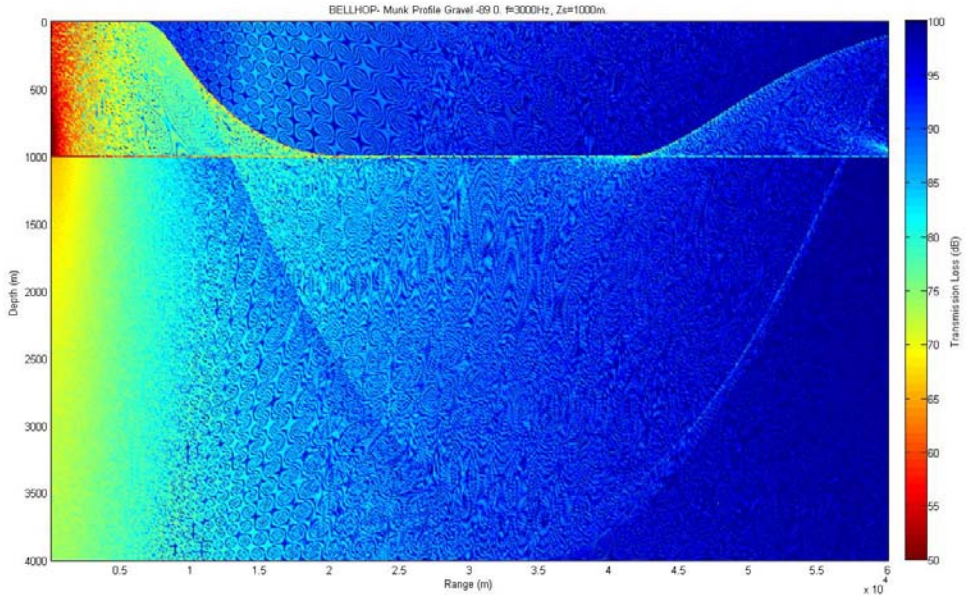

Figure 53. *TL* for a 3-kHz, 1000-m source in a 4000-m Munk sound speed profile

THIS PAGE INTENTIONALLY LEFT BLANK

VII. CONCLUSION

Existing networks, such as DART and Seaweb, have been used for wireless transmission of data underwater. Both have been able to relay data from a bottom-mounted sensor over long distances to a surface buoy. Both systems subsequently transmit the data via satellite to a shore-based site for further evaluation. A system such as Deep Seaweb combines attributes of these systems, and exploits RAP and DSC for military and civil long-range acoustic communications.

The Bellhop acoustic model provides a theoretical understanding of a deep-water acoustic network's effectiveness with variations of depth, sound-speed profile, and frequency. Given predictions of effective acoustic ranges, node placement can be optimized so an efficient number of nodes can be used for area surveillance and communications. The optimal placement of a sensor trying to exploit RAP is on or near the sea floor. In the DSC, the optimal node placement is at or just below the axis. The gateway node can connect either to a DSC node or to a seabed node. The operating frequencies of the acoustic modems should be as low as practical, while still retaining adequate spectral bandwidth. Recommend Deep Seaweb be developed with a communications band below 8 kHz, e.g., 5–7.5 kHz.

THIS PAGE INTENTIONALLY LEFT BLANK

LIST OF REFERENCES

[1] National Oceanic and Atmospheric Association Ocean Explorer. Text. http://oceanexplorer.noaa.gov/explorations/sound01/background/technology/media/iussnrl.html (accessed November 16, 2009).

[2] C. Meining, S. Stalin, A.I. Nakamura, F. Gonzalez, and H. Milburn. "Technology development in real-time tsunami measuring, monitoring and forecasting." In *Proc. IEEE OCEANS Conf.* vol.2, pp.1673–1679, September 2005.

[3] National Oceanic and Atmospheric Association National Data Buoy Center. Image. http://www.ndbc.noaa.gov/dart/dart.shtml (accessed November 13, 2009).

[4] National Oceanic and Atmospheric Association Center for Tsunami Research. Image. http://nctr.pmel.noaa.gov/Dart/ (accessed November 13, 2009).

[5] J. Rice and D. Green. "Underwater acoustic communications and networks for the US Navy's Seaweb program." *In Proc. SENSORCOMM '08 Conf.* pp. 715–722, August 2008.

[6] J. Rice, Deep Seaweb presentation, unpublished.

[7] R.J. Urick. *Principles of Underwater Sound*: *Third Edition*. Los Altos Hills, CA: Peninsula Publishing, 1983.

[8] R.J. Urick. *Sound Propagation in the Sea*. Defense Advanced Research Projects Agency, 1979.

[9] P-F. Piserchia, D. Rodrigues, J. Virieux, and S. Gaffet. "Detection of underwater explosion at very long range." In *Proc. IEEE OCEANS Conf.* vol. 2. pp. 698–702, September-October 1998.

[10] W.H. Munk and A.M.G. Forbes. Gloabal Ocean, "Warming: An Acoustic Measure?", *J. Phys Oceanogr*. vol. 19, pp. 1765–1778, November 1989.

[11] M. Ewing and J.L.Worzel. "Long-Range Sound Transmission," *The Geological Society of America Memoir 27 Propagation of Sound in The Ocean*. New York, NY: The Geological Society of America, 1948.

[12] P.M. Mikhalevsky, N. Dubrovsky, O. Godin, and K. Naugolnykh. "Obituaries Leonid Maximovich Brekhovskikh 1917–2005," *The Journal of the Acoustical Society of America*, vol. 118, no. 2. pp. 577–578, August 2005.

[13] W.H. Munk, P. Worcester, and C. Wunsch. *Ocean Acoustic Tomography*. Cambridge: Cambridge University Press, 1995.

[14] C.W. Ong. “A Discovery Process For Initializing Ad Hoc Underwater Acoustic Networks,” M.S. thesis, Naval Postgraduate School, Monterey, CA, 2008.

[15] J. C. Torres. “Modeling of High-Frequency Acoustic Propagation in Shallow Water,” M.S. thesis, Naval Postgraduate School, Monterey, CA, 2007.

[16] Curtin University of Technology Centre for Marine Science and Technology. Descriptive text and program, http://cmst.curtin.edu.au/products/actoolbox/ (accessed October 28, 2009).

[17] L. E. Kinsler, A. R. Frey, A. B. Coppens, and J.V. Sanders. *Fundamentals of Acoustics: Fourth Edition*. New York: John Wiley & Sons, Inc., 1999.

[18] F.B. Jensen, W.A. Kuperman, M.B. Porter, and H. Schmidt. *Computational Ocean Acoustics*. New York: Springer-Verlag New York, Inc., 2000.

[19] L. Brekhovskikh and Y. Lysanov. *Fundamentals of Ocean Acoustic*s. Berlin: Springer-Verlag, 1982.

[20] G.M. Wenz. “Acoustic Ambient Noise in the Ocean: Spectra and Sources,” *The Journal of the Acoustical Society of America*, vol. 34, no. 12, pp. 1936–1956, December 1962.

[21] W.H. Munk. “Sound channel in an exponentially stratified ocean, with application to SOFAR,” *The Journal of the Acoustical Society of America*, vol. 55, no. 2, pp. 220–226, February 1974.

[22] S. R. Thompson. “Displacement of Tethered Hydro-acoustic Modems by Uniform Horizontal Currents,” M.S. thesis, Naval Postgraduate School, Monterey, CA, 2009.

APPENDIX A. LLOYD'S MIRROR MATLAB CODE

```
clear all

r = [1:5000]; %receiver ranges (m)
f = 10; %frequency (kHz)
zs = 25; %source depth (m)
zr = 200; %receiver depth (m)
zbottom = 5000; %bottom depth (m)
c1 = 1500; %isovelocity sound speed (m/s)
c2 = 1800; %bottom sound speed
rho1 = 1024;% density of seawater (kg/m^3)
rho2 = 1843;% density of bottom (kg/m^3)
f1 = f*10^3; %frequency (Hz)

w = 2*pi*f1; %frequency (rad/s)
lambda = c1/f1; %wavelength in seawater(m)
k = 2*pi/lambda; %wave number
pref = 1; %reference pressure (uPa)
zsb = zbottom - zs; %changes reference point for bottom direct path
zrb = zbottom - zr; %changes reference point for bottom reflection

theta1 = atan((zsb+zrb)./r);
theta = pi/2 - theta1;
thetadeg = theta1 * 180/pi;

gamma1 = (w / c1) * cos(theta);
B = (w / c1) * sin(theta);
gamma2 = B .* sqrt(c1^2 ./ (c2^2 * (sin(theta).^2)) - 1);

R = (rho2 * gamma1 - rho1 * gamma2) ./ (rho2 * gamma1 + rho1 * gamma2); %bottom
reflection coefficient
Rphase = angle(R) ./ pi;

alpha = 3.3*10^-3 + [(0.11*f^2)/(1+f^2)] + [(44*f^2)/(4100+f^2)] + f^2*3.0*10^-4;
%attenuation coefficient (db/km)
alpha1 = alpha/1000; %attenuation coefficient (db/m)
alpha2 = alpha1/8.7; %attenuation coefficient conversion (Np/m)

R1s = sqrt(r.^2 + (zr-zs)^2); % surface direct path distance (m)
R2s = sqrt(r.^2 + (zr+zs)^2); % surface reflected path distance (m)
p1s = [exp(1i*k*R1s).*exp(-alpha2*R1s)]./R1s; %pressure caused by surface direct path
(uPa)
p2s = [exp(1i*k*R2s).*exp(-alpha2*R2s)]./R2s; %pressure caused by surface reflected
path (uPa)
ps = p1s-p2s; %total pressure (uPa)
```

```
TLs = -20*log10(ps/pref); %transmission loss with surface interaction (db)

R1b = sqrt(r.^2 + (zrb-zsb)^2); % bottom direct path distance (m)
R2b = sqrt(r.^2 + (zrb+zsb)^2); % bottom reflected path distance (m)
p1b = [exp(1i*k*R1b).*exp(-alpha2*R1b)]./R1b; %pressure caused by bottom direct path
(uPa)
p2b = [R.*exp(1i*k*R2b).*exp(-alpha2*R2b)]./R2b; %pressure caused by bottom
reflected path (uPa)
pb = p1b+p2b; %total pressure (uPa)
TLb = -20*log10(pb/pref); %transmission loss with bottom interaction (db)

%note p1s and p1b should be the same since they are both the direct path
%pressures from the source to the receiver

figure(1)
plot (r,TLs,'r');
title ('Surface Interference')
xlabel ('Range (m)');
ylabel ('Transmission Loss (dB)');
legend Bellhop Theoretical

figure(2)
plot (r,TLb,'k');
title ('Bottom Interfernce')
xlabel ('Range (m)');
ylabel ('Transmission Loss (dB)');
legend Bellhop Theoretical
```

APPENDIX B. MODIFIED IMPULSE RESPONSE MATLAB CODE

```
fid=fopen('RAPIR.arr');
for i=1:6
   tline=fgetl(fid);
end
xy=textscan(fid,'%f %f %f %f %d %d');
x=xy{3};
y=xy{1};
stem(x,y,'k.')
xlabel('Time (s)')
ylabel('Amplitude')
title('Impulse Response')
```

THIS PAGE INTENTIONALLY LEFT BLANK

INITIAL DISTRIBUTION LIST

1. Defense Technical Information Center
   Ft. Belvoir, Virginia

2. Dudley Knox Library
   Naval Postgraduate School
   Monterey, California

3. Professor Joseph Rice
   Naval Postgraduate School
   Monterey, California

4. Professor John Colosi
   Naval Postgraduate School
   Monterey, California

5. Professor Kevin Smith
   Naval Postgraduate School
   Monterey, California

6. Professor Daphne Kapolka
   Naval Postgraduate School
   Monterey, California

7. Professor Andres Larraza
   Naval Postgraduate School
   Monterey, California

8. Professor Fotis Papoulias
   Naval Postgraduate School
   Monterey, California

9. Professor Knox Millsaps
   Naval Postgraduate School
   Monterey, California

10. Dr. Charles Kimzey
    Naval Postgraduate School
    Monterey, California

11. James Ehlert
    Naval Postgraduate School
    Monterey, California

12. RADM Gerald Ellis (Ret.), USN
Naval Postgraduate School
Monterey, California

13. CAPT Carol O'Neal (Ret.), USN
Naval Postgraduate School
Monterey, California

14. CDR Jonathan Vanslyke, USN
Naval Postgraduate School
Monterey, California

15. LCDR Meng Chong Goh, Royal Singapore Navy
Naval Postgraduate School
Monterey, California

16. LT Jeremy Biediger, USN
Naval Postgraduate School
Monterey, California

17. LT Andrew Hendricksen, USN
Naval Postgraduate School
Monterey, California

18. LTJG Pongaskorn Sommai, Royal Thai Navy
Naval Postgraduate School
Monterey, California

19. ENS William Jenkins, USN
Naval Postgraduate School
Monterey, California

20. CAPT Mark Kohlheim, USN
SSC Pacific
San Diego, California

21. Mark Gillcrist
SSC Pacific
San Diego, California

22. Bill Marn
SSC Pacific
San Diego, California

23. Robert Creber
SSC Pacific
San Diego, California

24. Christopher Fletcher
SSC Pacific
San Diego, California

25. Paul Baxley
SSC Pacific
San Diego, California

26. Jerry Dejaco
SSC Pacific
San Diego, California

27. Paul Gendron
SSC Pacific
San Diego, California

28. Nancy Miller
SSC Pacific
San Diego, California

29. CAPT Dean Richter, USN
PMW 770
San Diego, California

30. CAPT Michael Byman, USN
NUWC
Newport, Rhode Island

31. Dana Hesse
Office of Naval Research
Washington, DC

32. Leroy Sverduk
Office of Naval Research
Washington, DC

33. Thomas Drake
NSWC Carderock
West Bethesda, Maryland

34. Harry Cox
Lockheed Martin
Bethesda, Maryland

35. Dale Green
Teledyne Benthos, Inc.
North Falmouth, Massachusetts

36. Edward Johnson
Chief of Naval Operations (N871B)
Washington, DC